University of Stavanger

Faculty of Science and Technology

MASTER'S THESIS

Study program/ Specialization: Petroleum Geosciences Engineering	Spring semester, 2015 Open
Writer: Emanuela I. Kallesten	…… (Writer's signature)
Faculty supervisor: Dr. rer. nat. Udo Zimmermann	
Thesis title: The North Sea Reservoir Chalk Characterization	
Credits (ECTS): 30	
Key words: North Sea, reservoir chalk, characterization, optical petrography, SEM, XRD, geochemistry, stable isotope geochemistry	Pages: 61 Stavanger, 15th of June, 2015

The North Sea
Reservoir Chalk Characterization

Author: Emanuela I. Kallesten

Supervisor: Dr. rer. nat. Udo Zimmermann

Master´s thesis presented to the

Department of Petroleum Engineering

Faculty of Science and Technology

University of Stavanger

June, 2015

ACKNOWLEDGEMENTS

First I would like to thank my supervisor, Dr. Udo Zimmermann for entrusting me with this unique and spectacular research project. Thank you for the trust; your guidance, support and encouragement during this project are much appreciated. But most of all, thank you for putting a rock in my hands, and for placing a graptolite under the microscope: I was sold!

I would like to thank my good friend and colleague Mona Minde, Ms. Ingunn Cecilie Oddsen and Ms Tania Hildebrand-Habel for the assistance with the cryo-SEM. I would also like to thank Dra Silvana Bertolino for her insight in the XRD process, and all the lab assistants diligently helping with sample preparation, posting, or traveling abroad with my samples.

To all my teachers, thank you for sharing the knowledge. Dear classmates, it´s been an honor to get to know each of you.

It couldn't have been done without the generous help of the sponsors. Thank you for taking the bill and I truly hope this research will pay off!

Finally, I would thank my entire family for all the sacrifices, their understanding and unconditional support. I dedicate this thesis to my husband and two wonderful children (mommy is going to cook dinner again now☺). Thank you for letting me live my dream!

TABLE OF CONTENT

LIST OF FIGURES

ABSTRACT

A significant amount of the hydrocarbon production in the North Sea is related to chalk reservoirs. Since 1969, the chalk play remains one of the most important oil sources in Norway. With the initial expected recovery factor 17%, development in technologies and methods contributed to a substantial increase in oil recovery to an approximately 40%. Much of the reserves in place are yet to be extracted, and secondary and tertiary recovery methods need to advance in order to mobilize the remaining hydrocarbons. An essential step in developing new enhanced oil recovery (EOR) methods is the understanding of the reservoir characteristics by thoroughly investigating the parameters influencing the EOR techniques.

This thesis contributes to the EOR research by using an array of analytical methods on core samples directly from one of the North Sea production oil fields, in order to provide a detailed characterization of the reservoir chalk.

Optical petrography shows a very fine, micritic carbonate matrix, with grains represented by various microfossils such as calcispheres, foraminifers, or sponge spicules. The XRD study confirms calcite as most abundant in the whole-rock composition, with quartz as an accessory mineral. The non-carbonate components consist mainly of quartz, but smectite, illite and kaolinite are also present. SEM micrographs indicate that the amount of clay minerals varies, increasing and diversifying upwards; they also show a clear decrease in porosity downwards, with more cementation and higher compaction.

The carbon and oxygen isotopic curves are consistent in throughout the sequence, with few exceptions, but the overall $\delta^{13}C$ and $\delta^{18}O$ are lower than the global isotopic curves expected for this period. The REE patterns are comparable to the typical seawater trends, but the Y/Ho ratios of an average of 36 are much below what is expected if fractionation would take place solely in seawater (above 90). The disturbing factors are interpreted as both clastic sediment input, and secondary fluid flow. The observed chemical differences between the cores do not

seem to reflect the flooding status.

Hence, reservoir chalk differs from most of the on-shore chalk (Hjuler and Fabricius, 2009), which compels caution when transferring results from the onshore chalk testing to reservoir chalk.

1 INTRODUCTION

1.1 "Oil from chalks, a modern miracle?"

Upper Cretaceous chalks are important reservoir rocks for hydrocarbon accumulation in the North Sea, embodying the beginning of the Norwegian oil adventure since the discovery of the Ekofisk field in 1969. The surprise of that discovery is well expressed in the rhetorical question of a 1977 paper written by P. A. Scholle: "oil from chalks, a modern miracle?".

Such unusually high porosity (40%) of chalk at a depth greater than 3000 m was unexpected and raised interest in the special circumstances that would make this possible, such as pressure conditions, chemical composition, burial history and oil generation and migration.

The chalk reservoirs proved to be among the most prolific hydrocarbon fields in the North Sea, Ekofisk field alone accounting for approximately 10% of the produced net oil equivalents on the Norwegian Continental Shelf (NCS) (source: npd.no).

A better understanding of the reservoir together with major advances in technology, lead to developing new and more effective recovery methods, so that the recovery factor increased from initially expected 17% to over 40%.

The golden era of giant oil fields discoveries is assumed to be a part of the past, and possible new fields are likely to be fewer and smaller. Therefore, developing Enhanced Oil Recovery (EOR) techniques has become a prioritized part of the national technology and research strategy for the petroleum industry, focusing on sustained profitability and resource optimization on the NCS.

Recent advances in EOR research encouraged setting the target for the recovery factor as high as 70%. If only 1% higher factor translates into a colossal economic potential, reaching that bold goal would not only revive the Norwegian oil adventure, but it would see it relive its golden days.

However, despite high-level production for the last 40 years, chalk plays are still relatively unexplored and little understood. Its complexity, as well as the way it radically differs from any other hydrocarbon play on the NCS, are some of the challenges in finding new, creative solutions for oil exploration, development, for reducing uncertainties and at the same time improve the oil recovery.

1.2 Objective

The target for the EOR techniques, also called tertiary recovery, is the remaining hydrocarbon capacity after the initial recovery, aiming to reduce the oil saturation at a microscopic scale (in the swept reservoir parts) as well as at a macroscopic scale (unswept areas).

EOR procedures include mainly miscible gas and fluid injections, chemical flooding, and thermal processes. Choosing the most feasible and efficient EOR technique for a specific reservoir is a key decision and it requires a thorough understanding of the reservoir parameters influencing the recovery factor, such as depth, pressure, temperature, lithology, porosity, permeability, wettability, fluid properties (hydrocarbon type, API gravity, viscosity), to name only a few (Gharbi, 2000).

In the quest of refining the techniques required for an increasing recovery factor in the North Sea, EOR research must perform extensive simulations on the chalk that resembles closest to the reservoir chalk in terms of its composition, petrography, diagenetic grade, and many other parameters that affect the rock –fluid interaction.

Although there are many studies conducted on reservoir chalk, there are very few published articles on the geological characteristics of such a reservoir.

By employing methods like optical petrography, X-ray diffraction, scanning electron microscopy (SEM) coupled with energy dispersive systems (EDS), and stable carbon and

oxygen isotope geochemistry, the study aims to characterize the individuality of the North Sea reservoir chalk in terms of its petrography, mineralogy, and geochemistry.

Hence, the major objective of the study is to describe thoroughly the composition and the texture of unflooded and flooded reservoir chalk.

So far never undertaken, this type of multidisciplinary analysis is one of the basic pillars of understanding the flooded onshore chalk for first comparisons of the reactivity of chalk when flooded with different fluids for EOR purposes.

2 THE NORTH SEA– Geological framework

The North Sea (Figure 1) is an intracratonic basin, formed as the result of several major tectonic events, which started in the Devonian and continued until Late Jurassic (appendix A). It covers an area of about 750,000 km^2 and shows some of the common structures related to extensional basins: horst-and-graben, rotated domino blocks, listric faults, and soft linked faults with different types of transfer zones (Bjørlykke, 2010).

Figure 1: Geographic location of the North Sea (*worldatlas.com)*

2.1 The North Sea basin - evolution through time (Ramberg, 2008)

The initial phase of basin formation is related to the Caledonian Orogeny, in the Devonian, when Laurentia collided with Baltica and Avalonia during the closure of the Iaepetus Ocean. Just before 400 Ma, when the compression ceased to act and its effect died out, the divergent plate movement took over and initiated the rifting between Greenland and Fenoscandia, process that eventually lead to the formation of the North Sea basin. During the Carboniferous, the compression of the Variscan mountain belt to the south lead to the developing of a vast foreland basin, parts of which are identified today in the southern segment of the North Sea. The basin was filled with large volumes of sand and mud, by continental depositional mechanisms, as most of the Norwegian sector of the North Sea was dry land.

Towards the Late Carboniferous, the climate of today´s central Europe changed from arid, equatorial, to more tropical, as a result of a northward continental drift. The humid climate favored the developing of a rich fauna and flora and thick coal beds of this age played a significant role as a source rock for the North Sea gas.

The Permian deposits are an important part in the stratigraphy of the region. Early to Mid-Permian thick sand packages, known as the Rotliegend Group, represent sand dune deposits in continental desert environments. Their name, derived from the German “Rotliegende - the underlying red”, refers to their particular red color due to the partial iron oxidation.

During the Late Permian, the arid climate continued to dominate the North Sea area, as well as fluctuating sea levels, linked to glaciation cycles. As the landmasses began to subside below sea level, and the basin became more isolated from the larger oceans, the shallow seas evaporated, resulting in the deposition of the Zechstein salt, mostly in the southern half of the basin.

The Triassic is characterized by further rifting, resulting in the expansion of the North Sea basin, and by the mobilization of the Zechstein salt, causing the occurrence of salt diapirs. The North Sea was still dry land, a broad alluvial plain, separating today Norway and Greenland. During an exceptionally arid climate, there was a high sediment input, mostly continental, transported by various types of river systems. The latest Triassic deposits are especially relevant as reservoir rocks, namely the Statfjord Formation sandstone. Just like the Permian Rotliegend Group, the Triassic sand strata have a distinct red color, and are commonly referred to as the "New Red Sandstone".

The main rifting phase in the North Sea occurred in the Jurassic. The northward drift continued, such that the climate became humid, tropical. By the end of Early Jurassic, the large alluvial plain was gradually submerged and the basin was filled with saline water. The transition from the red Triassic sandstones to the black marine mud deposits is an essential boundary for oil exploration. Middle Jurassic sedimentation was controlled by the great Brent Delta, resulting in some of the most prolific reservoir rocks in the North Sea. When the volcanism associated to the rifting eventually diminished, the entire region cooled down and experienced thermal subsidence. The Permian-Triassic rifting and normal faulting lead to the rotation of the basement and the overlying sediments, creating Domino-type fault blocks, with uplifted "shoulders", subject to erosion.

The Late Jurassic recorded an overall transgression and with it, the deposition of Mandal and Draupne Formations, a marine shale representing one of the most significant source rocks in the Central and Viking Graben. This is organic rich shale has a regional coverage in the North Sea basin, reaching a thickness up to 300 m.

In the Cretaceous, the prolonged rifting ceased, and was followed by a post-rift stage of thermal subsidence. During the Lower Cretaceous the base-level was still rising, setting an unique record of sea level height and temperature. Marls dominate the sediments of this age.

The most prominent deposits of Upper Cretaceous are the chalk of the Hod, Tor, and Ekofisk Formations in the southern part of the Central Graben. As this area became more isolated from terrestrial sediment supply, the deposits consisted mostly of clean calcareous muds, favored by the warm and sunlit water conditions. The deposition of chalk continued into the Cenozoic.

2.2 The North Sea Cretaceous Play

The Cretaceous play in the North Sea is represented mainly by the chalk reservoirs of Shetland Group (Hod, Tor and Ekofisk Formations) and Rogaland Group (Vidar Formation), located in the Central Graben and Utsira High. They are reworked, open marine sediments, with an Upper Cretaceous to Early Paleocene age. The source rock is the organic rich shale of Mandal and Draupne Formations of Late Jurassic age, and the trap is halokinetic and stratigraphic. Among the main representative fields are Ekofisk, Eldfisk, Valhall and Hod (Figure 2, source: NPD).

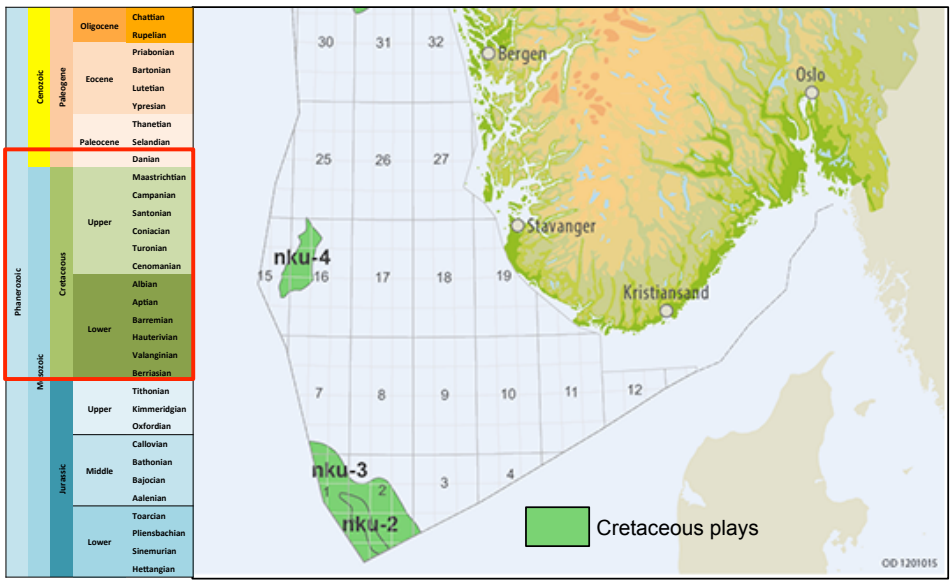

Figure 2: Distribution of the North Sea Cretaceous plays: nku-2 and nku-3 – southern tip of the NCS (Central Graben); nku-4 - Utsira High

2.3 North Sea Reservoir Chalk Formations

The most relevant reservoirs for the North Sea are Tor and Ekofisk Formations of Maastrichtian to Paleocene age, and Hod Formation (Mid-Turonian to Campanian, Figure 3).

The Hod Formation consists of grey, partly pink to red, fine-grained argillaceous chalky limestones and varies in thickness between 200 and 700 m. At the bottom of the formation prevails clean chalk, which often forms a reservoir, while towards the top of the succession, the amount of clay increases. Most of the chalk is laminated and burrowed, but grainstone turbidites are also common.

The conformably overlying Tor Formation consists typically of homogeneous white to pale grey chalk with few chert nodules or layers. Its thickness is mostly less than 150 m, but can increase up to 250 m in depocenters. The formation contains several facies including hardgrounds, pelagic chalk, allochthonous deposits, and shallow marine chalk.

The hydrocarbon-rich Ekofisk chalk is mainly grey to white with partly significant amount of stylolites and has rarely developed layering (source:NPD).

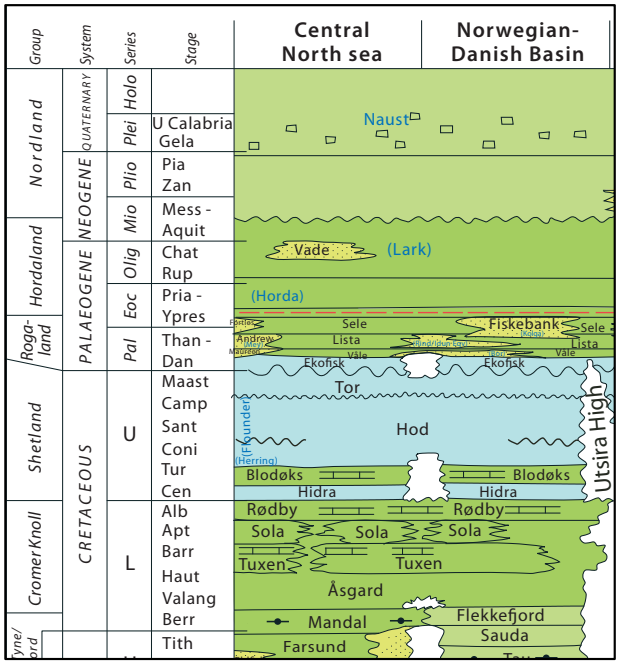

Figure 3: Excerpt from NPD´s lithostratigraphic table, showing the Hod, Tor, and Ekofisk Formations´distribution in the Central North Sea and Norwegian Danish Basin (legend and further details are shown in Appendix A)

3 CHALK

3.1 General Classification

A general description defines chalk as a marine, well-cemented biomicrite, formed mainly by the debris of planktonic organism known as coccolithophorids.

Mineralogically, it consists mostly of calcite, but also a various percentage of clay minerals, authigenic glauconite, as well as apatite. Silica is often found in chalk deposits in varying quantities, from small diatoms, or radiolarian skeletons, to nodules, or beds of chert (Bonewitz, 2005; Kennedy, 1985).

The general classification according to the depositional texture of carbonate rocks places chalk at the fine-grained end of the chart, between mudstone and packstone (Figure 4), while according to Folk classification of textures in carbonate rocks, chalk is a micrite or a fossiliferous micrite.

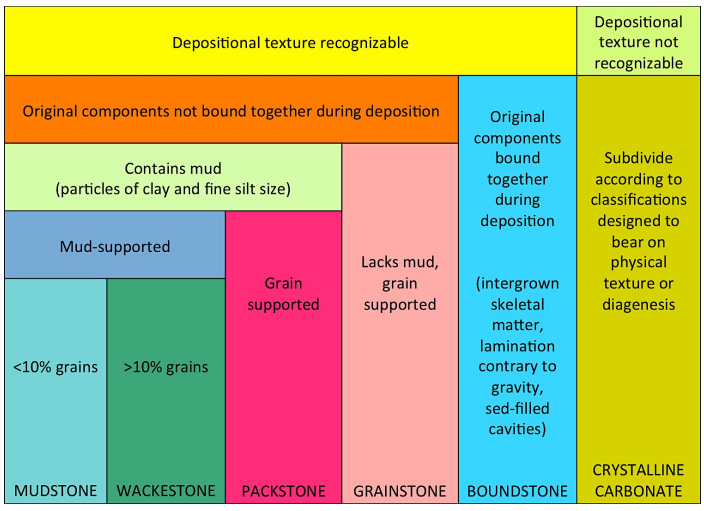

Figure 4: Dunham classification of carbonate rocks according to the depositional texture (Dunham, 1962)

However, a general classification as such is mostly descriptive, intended to address certain aspects of interest, and does not always comprise the lateral and stratigraphic variations found very often in chalk units as the ones in the North Sea.

3.2 Sediment composition

The main component of the chalk is the matrix, consisting of nanofossil mud background with less than 0.03mm grain size, not visible to the human eye, representing whole, or fragments of coccolithophorids. The skeleton of these organisms is referred to as coccolith and is formed by calcite tablets (platelets) organized radially, into rosettes or rings, up to 20 μm diameter. In turn the rosettes form a hollow coccosphere, which protects the soft part of the organism (Figure 5). The distinction between the coccolith groups is mostly related to the shape of the constituent platelets and the structure of the coccosphere (Kennedy, 1985).

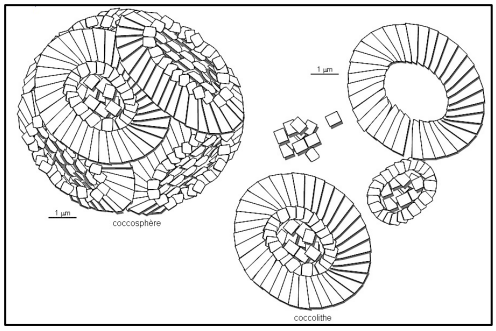

Figure 5: Typical Jurassic-Maastrichtian assemblage of calcite platelets forming the coccolith and coccosphere (Banque de Schemas)

In addition to the nannoplankton, the chalk matrix may include clay minerals and traces of quartz.

Grains are present in a much smaller proportion and represent skeletal fragments of microfossils, calcispheres, foraminifera, bivalvia, brachiopoda, porifera, or crystals with sizes large enough to be visually observed in the rock.

Calcispheres are small, initially hollow calcite spheres, between 30-400 μm, common for deep-water sediments, and arguably represent algal remains (cysts). Difference in wall structure discriminates between varieties of calcisphere types; one of the most common is the Stomiosphaeriadae, which consists of radial calcite prisms, arranged radially in a single layer, up to 15 μm long (Kennedy, 1985).

Foraminifera are benthic and planktonic organisms, and are a common occurrence in chalk units. They form chambered shells (tests), which vary from 0.1 to 1 mm in size. The test wall composition and microstructure, as well as the internal morphology of the organism make the distinction between different foraminifera groups (Figure 6, Flügel, 2004).

Their importance is generally recognized as time markers for biozonation of marine carbonates, they provide insight in the ancient depositional systems and microfacies analyses.

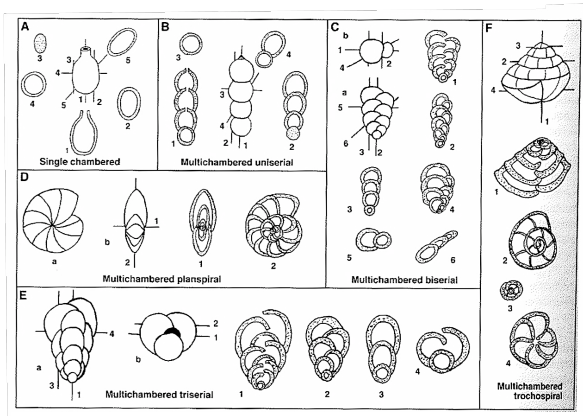

Figure 6: Classification of foraminifers according to their chamber arrangement

Sponges (Porifera) are benthic organisms, divided into two major groups: siliceous and calcareous. The skeleton (spicules) differs between the different sponge types by the number of axes and rays in which they are organized (Figure 7). The siliceous skeletons found in carbonate rocks are dissolved and entirely or partially calcified (Flügel, 2004).

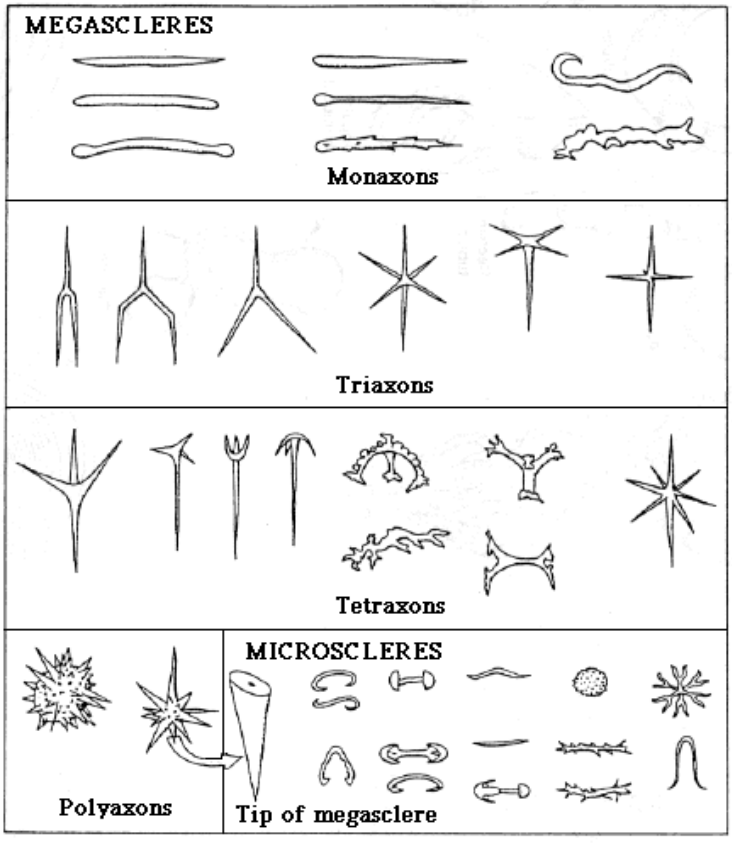

Figure 7: Proposed nomenclature of sponge spicules, addressing the size, number of rays and axes (palaeos.com)

4 SAMPLING AND METHODOLOGY

4.1 Data set

The study is performed on core samples of reservoir chalk from the North Sea.

A total of 12 of the cores from an active production well represent cut plug samples cored parallel to the core axis, 1.5” (approximately 4 cm) in diameter and between 75-80 mm long. The core depths range from 16154 ft to 16100 ft,

These are sectioned (cut in the lab) in several smaller fragments, labeled according to the method for which they will be used, and ready for further processing.

4.2 Sample ID

Sample identification is primarily based on the stratigraphic depth of the cores, using cardinal numbers, 1 being the shallowest. Further, they are differentiated by the flood status that each of the cores has previously undergone.

Unflooded*	UF
Waterflooded**	WF

* core plugs from horizons that have not undergone improved oil recovery processes
**flooding status referring to seawater injection (waterflooding), one of the main techniques for secondary oil recovery

Samples 1 to 5 and sample 12 are unflooded, and samples 6 to 11 are waterflooded. An overview of the cores used in this project is shown in appendix B.

4.3 Optical petrography – UiS

Optical petrography is a preliminary method used for revealing first data about the texture and the composition of the chalk. The optical microscope utilizes visible light in order to produce a magnified image of a study object´s surface, by focusing the light scattered from the specimen through a succession of lenses.

4.3.1 Sample preparation

The samples to investigate are polished thin sections, cut and prepared in an external laboratory. The analysis involved examining the samples by using a Zeiss AXIO polarized light microscope, procedure that took place at the University of Stavanger. The micrographs are taken with an AxioCam ERc 5s camera, connected to a computer.

4.3.2 The light microscope

The method takes advantage of the dual behavior of visible light, both as particles (photons) and as waves, consisting of oscillating electric (E) and magnetic (B) fields. The two components oscillate as a sine function of space and time, so that at any given instant, or location, they are represented by vectors of equal amplitude and phase, moving in two mutually perpendicular planes (Figure 8). Their wavelength and frequency is determined by the particular energy associated with the photons (Murphy, 2013).

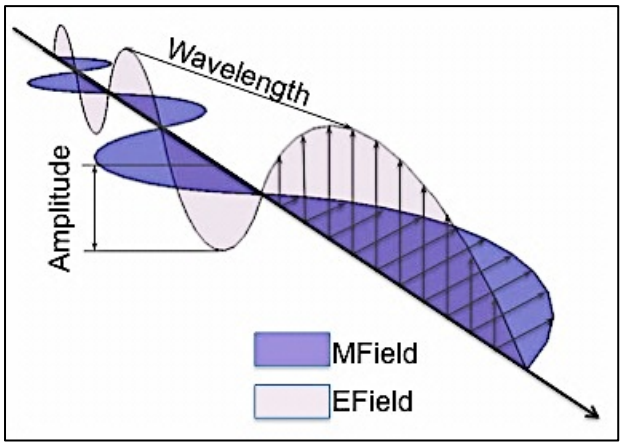

Figure 8: Graphic representation of electromagnetic wave propagation in a direction that is always at a right angle to both the electric and the magnetic vibrating field vectors

The bulk source light used in light microscopes is nonpolarized (i.e.: E waves vectors vibrate at any possible directions). An essential application value of the light microscope is enhancing the contrasts in the sample by imaging it under polarized light, where the E vectors of all the waves no longer have a random orientation, but vibrate in a single plane (Figure 9). The linearly polarized light is obtained by incorporating two filters, a polarizer, and an analyzer, set to be at a right angle to each other. The polarizer is placed below the specimen on a rotatable holder, while the analyzer is above the sample stage and it can be removed from the path of the light. By removing the analyzer, the sample is seen in plane-polarized light, while by inserting the analyzer, the sample is observed with crossed polars (MacKenzie, 1994).

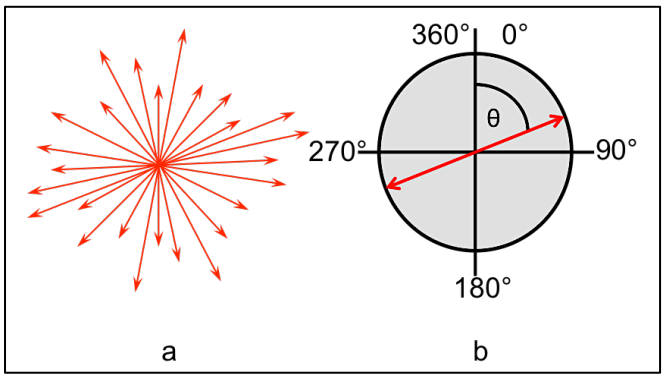

Figure 9: Schematic cross section of two light beams, looking along the beam propagation axis. (a) random lvector orientation and various wave amplitude; (b) linearly polarized light with single plane vector orientation (after Murphy, 2013)

Polarized light interacts in a direction-sensitive manner with the crystals, so that the produced image helps identifying of crystalline minerals in the specimen (Murphy, 2013). In case of calcite, due to its birefringence, it reflects as subtle pastel interference colors when seen with cross polars. The color shades change as the sample stage rotates, as well as the relative relief of individual crystals, emphasizing crystal morphology twinning, crystal cleavage, or zoning. A similar and corroborative effect has the rotation of the polarizer between 0° and 90°.

The light microscope resolves particles down to 0.2 microns, as it is limited by the wavelength of the visible light. The resolution uncertainties are related to factors like wavelength of the light source, specimen quality, or lens quality (Murphy, 2013).

4.4 Scanning Electron Microscopy (SEM) - UiS

A scanning electron microscope is a valuable instrument for producing high-resolution images of the surface topography, the slightly deeper lying mineralogy via electron excitation with back-scattered electron detection and semi-quantitative, chemical composition via X-ray measurement.

Because the cores are assumed to be wet sedimentary rocks, the analysis requires constant cooling of the system with liquid nitrogen, a special procedure called cryo-SEM.

The analysis took place at the University of Stavanger, on a Zeiss Supra 35VP scanning electron microscope, equipped with a Polar Prep 2000T cryo-SEM system.

4.4.1 Sample preparation

A total of five samples are examined with cryo-SEM, two unflooded and three that were flooded. The samples are small, inner core fragments of millimeter scale, and mounted on a copper holder. Lowering the samples into nitrogen slush (i.e., liquid nitrogen cooled under vacuum conditions) ensures rapid freezing, measure taken in order to avoid the vaporization of the hydrocarbons during electron scanning, and consequently contamination of the SEM column.

Before transferring the samples into the SEM chamber, they are sputter coated with platinum; the coating increases the conductivity of the sample, protects the sample from damage during the process, counters the electrical charge that builds up under the electron radiation, and not the least, enhances the secondary electron emission and thus provides better image resolution.

4.4.2 The SEM process

The samples are enclosed in a vacuum chamber. Electrons from the filament are accelerated through a potential field and focused into a thin beam with the help of the three lenses, onto the sample surface (Figure 10). Scanning coils placed between the last two lenses direct the electron beam to scan in a raster pattern. As the beam electrons interact with the sample,

primary (higher energy, elastic scattering) and a number of secondary (lower energy, inelastic) processes result in electron emissions. These responses are detected and transmitted through deflection coils into a cathode ray tube, where the image is analog, but enlarged.

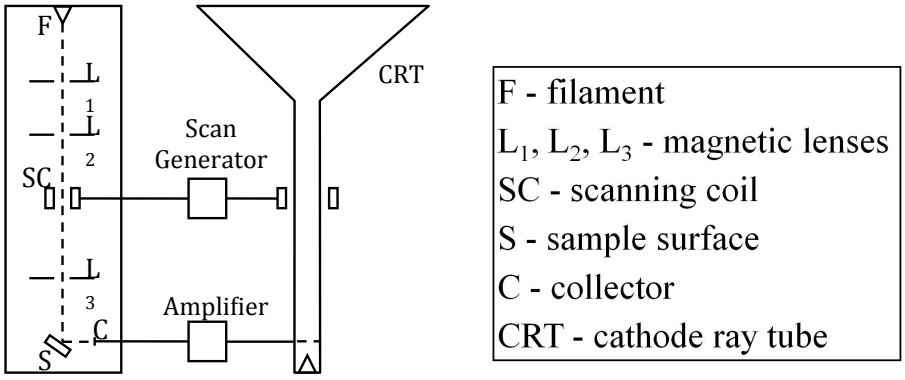

Figure 10: Schematic principle of the SEM, after J. Hjelen, Metallurgisk Institutt, NTH

4.4.3 Backscattered Electrons

The interaction of the electron beam with the sample target produces a number of elastic collisions between electrons and atoms within the sample, referring to the electrons that instead of being absorbed are scattered out of the target. The volume of backscattered electrons is proportional to the target´s atomic number, i.e. the greater atomic number, the more likely to produce a more elastic collision and therefore generate more backscattered electrons (Goldstein, 1981).

The integrated BSED is is placed above the sample in the sample chamber. Since backscattered electrons reveal compositional contrasts, the interpretation of the grey tones in the generated image associates the stronger BSE intensity, due to elements with a larger atomic number, to lighter shades, whereas the dark areas point out to lighter elements. The contrast between the different shades of grey is best seen when the sample is perfectly flat; in an inclined surface, heavier elements can be overshadowed and appear similar to the lighter ones, so that compositional contrasts may be overlooked. Uneven sample topography can also reduce image accuracy.

Because the beam electrons penetrate some microns into the solid sample, the emerging backscattered electrons provide information about the slightly deeper lying mineralogy of the sample.

4.4.4 Secondary Electrons

The energy from the beam electrons that is deposited in the sample generates secondary electron emissions, the effect of inelastic scattering. Specific for secondary electrons is their shallow sampling depth, related to the low kinetic energy.

Compared to the backscattered electrons, secondary electrons are insensitive to the atomic number, but their intensity varies with the angle of incidence between the beam and the sample. This variation is the result of the changes in the sample topography (Goldstein, 1981). The intensity of the detected signal controls the light strength on the cathode ray tube, synchronizing each spot on the sample surface where the electrons were detected to corresponding pixel on the obtained image. In this way, the image represents a highly accurate distribution map of the detected signal strength, and in consequence the sample topography.

4.4.5 X-ray emissions

Also related to inelastic scattering, energy-dispersive x-ray spectrometry (EDS) provides semi-quantitative information on chemical composition. During the beam electrons and sample interaction, electrons from the inner shell of the atoms are ejected, their place being taken by higher energy electrons from the outer shell. This transition causes a change in energy, which can generate characteristic x-rays, specific to elements that emit them. The detection process involves the proportional conversion of the photon energy into an electrical signal, amplified and sent to a multichannel analyzer (Goldstein, 1981). The EDS system records the number and the intensity of the signal, and displays them in electron volt units

versus counts. As the signal is specific to the atomic structure and distribution, the spectra are a unique combination of peaks, graphically representing the chemical composition of the sample.

The resolution of the spectra increases with increased amount of time used for processing each pulse, although the spectral resolution is rather low (130-150 eV). Because EDS measures all the emitted x-rays simultaneously, it does not provide accurate quantitative analyses.

4.5 XRD - Outsourced

X-ray diffraction (XRD) is one of the most reliable methods for mineralogical analysis. When performed on whole-rock samples, it provides information about the mineral composition of the sample, while a study on the mineral separates helps identify and quantify the clay mineral content (Emery, 1993).

X-ray diffraction from single crystals resolves molecular structures to an atomic resolution. Also a form of electromagnetic radiation, the X-rays have a much higher typical photon energy than the visible light, and their wavelength is comparable to the interatomic distance within crystals.

The principle of XRD as an analytical method lies in Bragg´s law (Figure 11) and it refers to the inversely proportional relationship between the X-ray angle of diffraction and the characteristic spacing between a regular array of parallel layers (Emery, 1993).

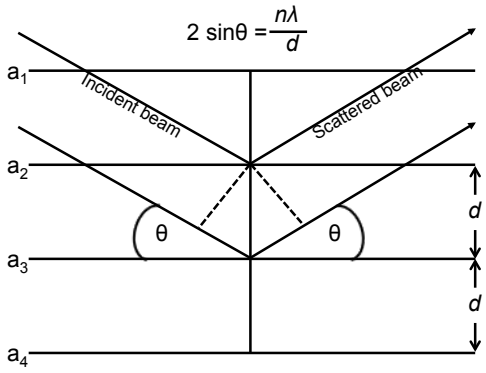

Figure 11: Illustration of Bragg´s law of diffraction. An incident beam of X-rays that hits the array of reflecting planes at an angle θ is reflected at the same angle. a_1, a_2.. are lattice arrays of atoms assumed to be a stack of parallel planes, equally spaced at a distance *d; n* is the integer number of the wavelength λ of the incident beam

4.5.1 Sample preparation

For the whole-rock investigation, the XRD analysis uses powder samples of very fine silt and clay particle size, hand-milled in order to avoid the damaging of the crystals. Using an agate beaker for milling is a measure to avoid sample contamination.

For analyzing the XRD of the non-carbonate content, a separate core fragment is first milled, and then dissolved in acetic acid. When all the calcite is dissolved and all that is left is the non-carbonate fraction, the liquid is emptied slowly, making sure that the separated material is not wasted. Centrifuging the sample for a few minutes will remove most of the liquid. Finally, the material is set in the oven for several days, to dry completely. The entire sample preparation is time consuming, but a thorough procedure should result in a calcite-free sample material. A drop of HCl solution on the sample should give no reaction.

4.5.2 The XRD process

A small amount of powder is placed into a metal cavity mount holder, with a pressure sensitive tape.

The X-ray source is set in such a way that the produced beam consists of X-rays of known wavelengths. These are filtered to generate radiation of a single wavelength (monochromatic),

directed towards the sample. The sample is then rotated in the beam until the diffracted ray paths reach an appropriate angle.

When the beam of X-rays hits an ordered array of reflecting planes at a certain angle θ, the reflection angle is equal to the incidence angle θ. The premise of the method is that crystals are a stacking of repetitive units with specific lattice motifs, at a regularly spaced interval *(d)*, forming parallel planes, and with a morphology given by the size and shape of the units, as well as their type of symmetry (Van Holde, 2006).

As each crystal has a unique, specific structure, the diffracted X-rays follow a path representative to the particular geometry and dimensions of the unit cell of the lattice, while the intensity of the scatter is a reflection of the atomic distribution within the crystal.

The outcome of the measured diffraction is spectra of *d* versus number of counts, with unique combinations of peaks as a fingerprint of the crystal structure. In this way, an interpretation of these spectra makes a clear discrimination between minerals with similar chemical composition possible (Emery, 1993). The width of the peaks is a reflection of the instrument´s analytical error; the smaller the grain, the higher the uncertainty.

4.6 Isotope geochemistry - Outsourced

Studies on the oxygen and carbon stable isotopes in carbonates are often used to gain insight in the depositional environment, ambient pH, salinity, the paleoclimate, or paleo-water temperature. Carbon and oxygen are main constituents of not only carbonate rocks, but also of most forms of life. They are fairly light elements, the relative mass difference between their more abundant light isotopes and the heavier, less abundant isotopes is prominent, a property that is favored in stable isotope interpretation. Moreover, the least common isotope is abundant enough for accurate analysis.

4.6.1 Isotopic fractionation

To the ground of stable isotope geochemistry is isotopic fractionation, referring to the partitioning of isotopes of an element, leading to the enrichment of one isotope relative to another. The change in isotopic ratios is mostly a function of the strength of chemical bonds, in its turn affected by the mass difference between the isotopes. Generally, heavier isotopes form slightly stronger bonds than the lighter isotopes. In natural systems, this leads to two main fractionation types: kinetic fractionation (isotopic exchange during bio-chemical reactions) and equilibrium fractionation (the effect of variations in the thermodynamic properties of the isotopes) (Misra, 2012; Emery, 1993).

The stable isotope ratios are calculated in terms of their deviation from the corresponding ratios of a known, internationally accepted standard and it is expressed as delta (δ) values in units of parts per mil (‰), according to the equation below, exemplifying the carbon isotope calculation:

$$\delta\,^{13}C = \left[\frac{13C/12C(sample) - 13C/12C(standard)}{13C/12C(standard)}\right] * 1000$$

The standard used in this study for comparison of both the carbon and the oxygen compositions is the V-PDB (Vienna Pee Dee Belemnite).

4.6.2 Mass Spectrometry (MS)

A mass spectrometer separates and detects ions of slightly different masses, so that in the case of molecules like carbon dioxide (CO_2), it easily identifies and quantifies the carbon and oxygen isotopes and their ratio.

The analyses took place at the Wolfson Laboratory, School of Geosciences Grant Institute, Edinburgh University. The sub-samples were reacted with pure orthophosphoric acid at 90° in an ISOCARB automatic carbonate preparation system, and the resulting carbon dioxide was analyzed in a VG Isoglas PRISM III stable isotope ratio mass spectrometer.

4.6.3 Sample preparation

The probes for mass spectrometry are in the form of fine powder obtained by drilling small cavities on various core surfaces. As the sensitivity of the mass spectrometer is very high, 0.5 grams of powder are sufficient for accurate analysis.

After each drill, the used heads were cleaned with acetone, to avoid cross contamination.

4.6.4 The MS process

The basic analytical procedure in mass spectrometry includes machine preparation, chemical separation of the element of interest, ionization of molecules, quantitative detection of mass spectra and computation of isotope ratios.

First, the carbon and oxygen molecules are chemically separated, by dissolving the samples into 100% orthophosphoric acid, a reaction resulting into carbon dioxide (CO_2). Once the sample is entirely dissolved (ca 5 min), the CO_2 is purified and concentrated by repetitive freezing and thawing of the gas.

The next step in the process is the ionization of the gas. The CO_2 is exposed to an electron beam; as the gas molecules start losing electrons, the positive charged ions are retrieved from the electron beam by a powerful electromagnet and separated according to their mass, ready to be collected. The machine is calibrated to only pick up the masses of interest, in this case 44, 45 and 46, given by certain isotope combinations.

$$44 = {}^{12}C\ ,\ {}^{16}O\ ,\ {}^{16}O$$
$$45 = {}^{13}C\ ,\ {}^{16}O\ ,\ {}^{16}O$$
$$46 = {}^{12}C\ ,\ {}^{16}O\ ,\ {}^{18}O$$

The ratios of interest are ${}^{18}O:{}^{16}O$ and ${}^{13}C:{}^{12}C$. Dividing mass 45 to mass 44 results in ${}^{13}C:{}^{12}C$. Further, mass 46 divided by mass 44, will cancel out the carbon, being left with the ${}^{18}O:{}^{16}O$ ratio.

These masses, once identified and quantified, produce a specific voltage that converts into an optical signal. A computer registers the signal and generates a digital file, which contains all the raw data and the measured parameters for each sample. The data is then summarized and ready for interpretation.

4.6.5 Oxygen system

Oxygen isotope fractionation is mainly the effect of equilibrium processes, and the enrichment of the ^{18}O isotope in calcium carbonate relative to the seawater is a function of temperature. Therefore, oxygen isotope studies are often applied to estimating temperatures of ancient oceans.

Anderson and Arthur (1989) propose a direct proportionality between the $\delta^{18}O$ and the ambient temperature:

$$T(°C) = 16.0 - 4.14\ (\delta_c - \delta_w) + 0.13\ (\delta_c - \delta_w)^2$$

where δ_c is the $\delta^{18}O$ PDB composition of the sample, and δ_w represents the $\delta^{18}O$ SMOW (Standard Mean Ocean Water) composition of the ambient sea water (in this study assuming a -1‰ value, typical for non-glacial oceanic water).

4.6.6 Carbon system

As opposed to oxygen, carbon isotope fractionation is fairly independent from temperature changes, so that carbon isotope ratios are mainly an indication of the source of carbon in the carbonate cements.

The most abundant stable carbon isotope is ^{12}C (98.89%), while ^{13}C represents 1.11%. Organic carbon is typically enriched with the light isotope. As it forms weaker, more easily broken bond, organisms would preferentially use the lighter C-isotope. Therefore, in kinetic

processes like photosynthesis, the lighter isotope is favored to the heavier, and it becomes more concentrated in the produced organic matter, implying more negative $\delta^{13}C$ values.

The equilibrium fractionation processes, like dissolution of carbon dioxide in seawater and reprecipitation of carbon, are more temperature-dependent and lead to enrichment in ^{13}C of seawater and marine carbonates at a minor scale (Rollinson, 1993).

4.7 Geochemistry - outsourced

Geochemistry is an important tool in petroleum research that quantifies the abundance of major and trace elements. When used with the inductive coupled plasma linked with mass spectrometry (ICP-MS) technique, it will identify all major elements and more than 45 trace elements to describe and to interpret the geochemical composition of chalk.

Geochemical data analysis took place at Acme laboratory (Vancouver, Canada).

4.7.1 Sample preparation

The analysis is performed on a significant fragment of the core sample. For accurate results and in order to avoid analytical artefacts, it should represent unweathered and clean surfaces, neither affected by visible secondary fluid flow, nor containing veins.

30-40 g of the core fragment are first broken into granules. Further, the material is machine milled in an automated, ultra clean agate mill at the University of Stavanger. The subsamples are pulverized to a fine mesh in a Retsch RS200 milling machine, for 2-3 min at 700rpm.

The geochemistry analysis of the clay content is performed on the remaining material prepared for XRD.

4.7.2 The ICP-MS process

The ICP-MS system includes the nebulizer (sample introduction system), the ICP torch, a high frequency generator, and finally the mass spectrometer linked to the computer.

The method requires that the samples to be analyzed are in solution before they are introduced into the ICP torch. The inductively coupled argon plasma is used as an atomic emission source. The light that the atoms, or ions emit is picked up by a photomultiplier and then converted to an electrical signal in the mass spectrometer. The intensity of this signal is the base of element concentration calculations, by comparison with a known standard (Thompson and Walsh, 1989).

Because detection limits are in general very low, and complete multielement analysis can be achieved simultaneously in a short period of time, this is one of the most reliable and used analytical methods.

Detection limits and detailed description of the analytical process and certificates used for this project can be downloaded under http://acmelab.com.

5 RESULTS

5.1 Optical Petrography Results

A common characteristic for the 10 studied thin sections is the very fine carbonate micritic matrix consistent with the general chalk description. The matrix is beige, with tone variations that can be associated either to stratigraphic changes, composition, or to the different thickness of the specimens. Although the resolution of the light microscope does not allow for a thorough textural description of the matrix, it can be defined as generally homogeneous, without visible layering.

The grains vary between 10-100 μm, and represent calcispheres, various types of foraminifera and sponge spicules (Figure 12).

The sponge spicules are predominantly white elongated rays (monaxone) or triods (triaxone). The amount of spicules varies between the thin sections; they have different sizes, most likely as a result of specimen sectioning (Figure 12a, b); they show a preferred orientation, oblique to the core axis, indicating transportation. Most of the spicules seem to be cemented with calcite.

All thin sections contain calcispheres and foraminifers, recognized by their circular calcite rim. Some of them are completely cemented with calcite (Figure 12c, e), some contain fairly large precipitated crystals (Figure 12d), while others seem to be hollow. This is common for all thin sections, from both unflooded and flooded cores. Some sections contain a local accumulation of calcispheres.

Present in all thin sections are circular, micron scale features, without a rim, which appear black or opaque in the micrographs; most of them are perfectly rounded, although elongated shapes are also present. Such reflections are typical for organic matter, but can also represent opaque minerals. The same opaque reflection can be seen in larger areas (Figure 12c, f) of over 100 microns, where the matrix is almost, or entirely absent. It is most likely a secondary feature, as it seems to enclose other sedimentary grains, but at the same time overlap the dark pore spaces. Whether this is indeed trace of hydrocarbons, mineral precipitation, or merely pores filled with resin from the preparation process can be further investigated with other methods.

Fractures are seen in most of the thin sections (Figure 12f). They are filled with the same opaque material, assumingly organic matter.

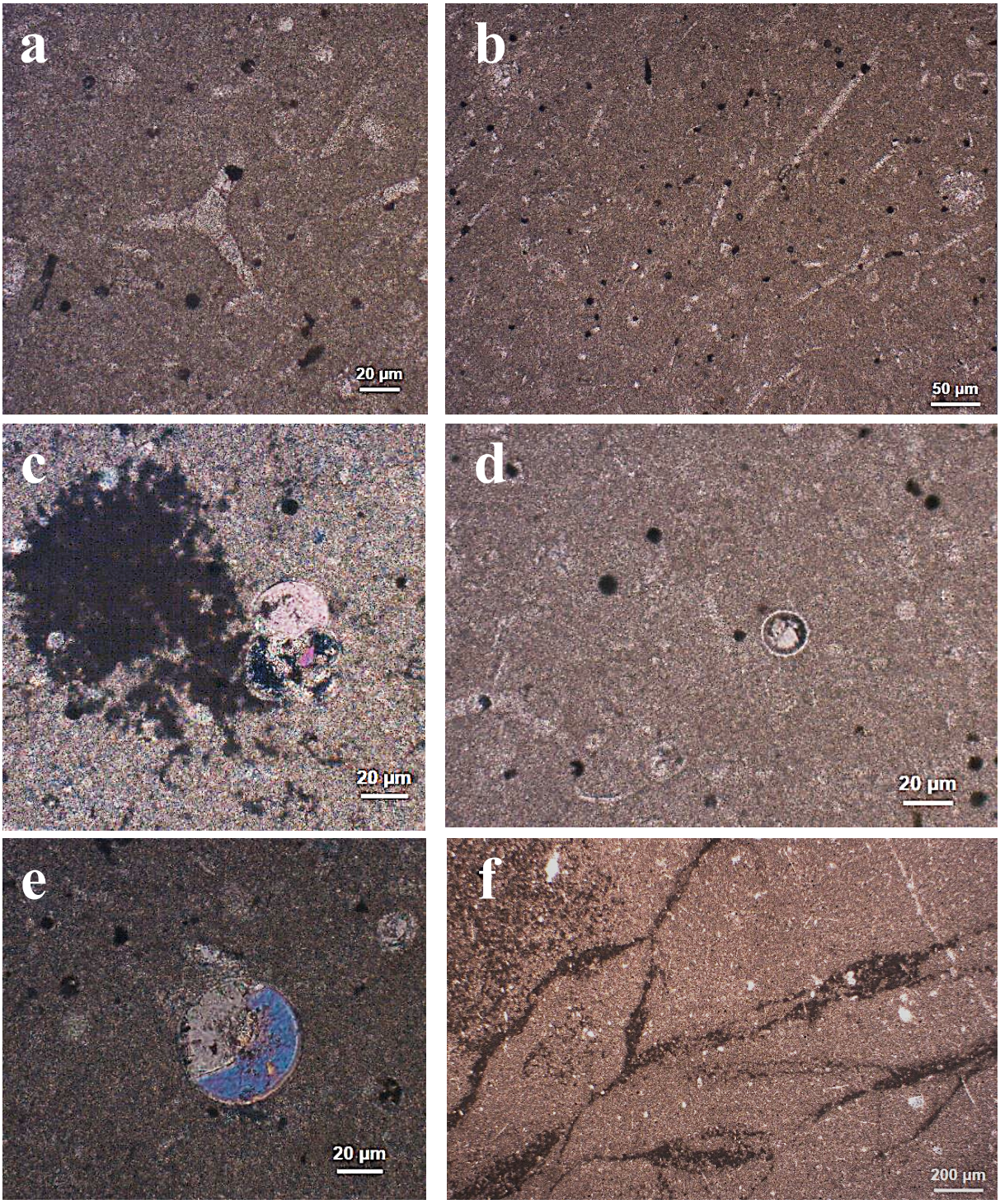

Figure 12: Micrographs of reservoir chalk thin sections with light, beige macritic matrix, microfossils and opaque features. (a) triaxone sponge spicule, core 4UF; (b) larger area of 4UF showing the high concentration of white, elongated sponge spicules (monaxones) most likely calcified; (c) a large area representing an opaque material; to the right, multichambered foraminifer partially filled with calcite (sample 5UF); (d) calcisphere (center) with calcite rim and containing precipitated mineral, calcite, or possibly dolomite ; (e) calcisphere seen with crossed polars and reflecting calcite cement (5UF); (f) interconnected microfractures seen in sample 2UF, and filled with an opaque material

5.2 Scanning Electron Microscopy Results

The Secondary Electron Microscopy revealed further characteristics of the morphology of the reservoir chalk.

5.2.1 Unflooded chalk

Sample 12UF lies lowest in the stratigraphy. The SE images show a fine-grained carbonate rock, consisting of mostly of coccoliths. Although the majority are fragmented, whole coccoliths are present, as well as unbroken coccospheres (Figure 13a, b).

Many of the calcispheres are broken, some are filled with coccolith debris, and some contain growing calcite crystals (Figure 13c, d).

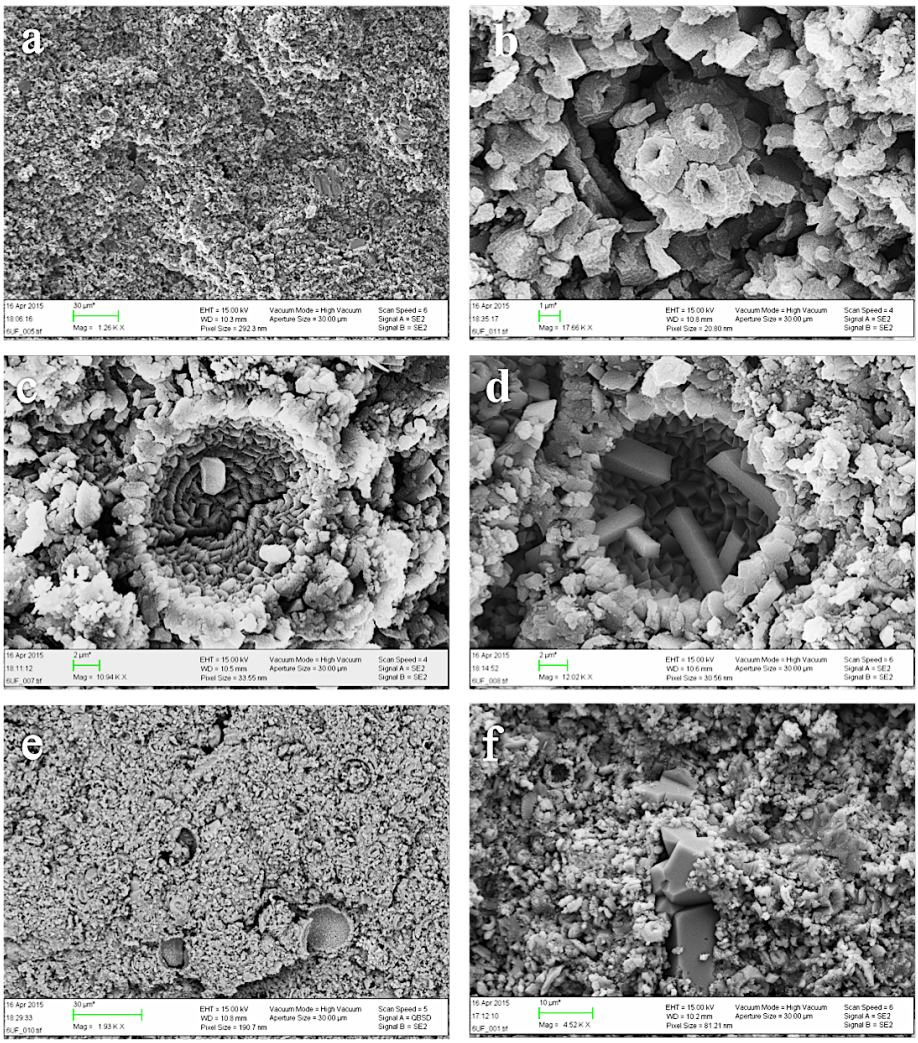

Figure 13: SEM micrographs of sample 12UF: (a) overview of the sample surface; (b) whole coccosphere in the matrix; (c) broken calcisphere; (d) calcipshere containing precipitated calcite; (e) BSE image of the sample surface showing a very homogeneous mineral composition; (f) calcite precipitated in situ (center) and calcite cement (to the right)

An overview of the sample surface under the BSE detector shows a very homogeneous mineral composition, with calcite represented in a very high proportion (Figure 13e). The few, small, lighter grey tones represent flakes of clay minerals. Most of the crystals in the sample are large calcite crystals; Figure 13f shows a growing calcite crystal, with very clear, sharp edges, indicating in situ precipitation. Calcite cement is also common.

Besides calcite and the clay minerals, halite is also present (Figure 14). Halite is an evaporite mineral, recognized by the cubic crystal shape, it is soluble in water, and it has a saline taste. The large, perfect crystal in this sample has the characteristics of in situ precipitation.

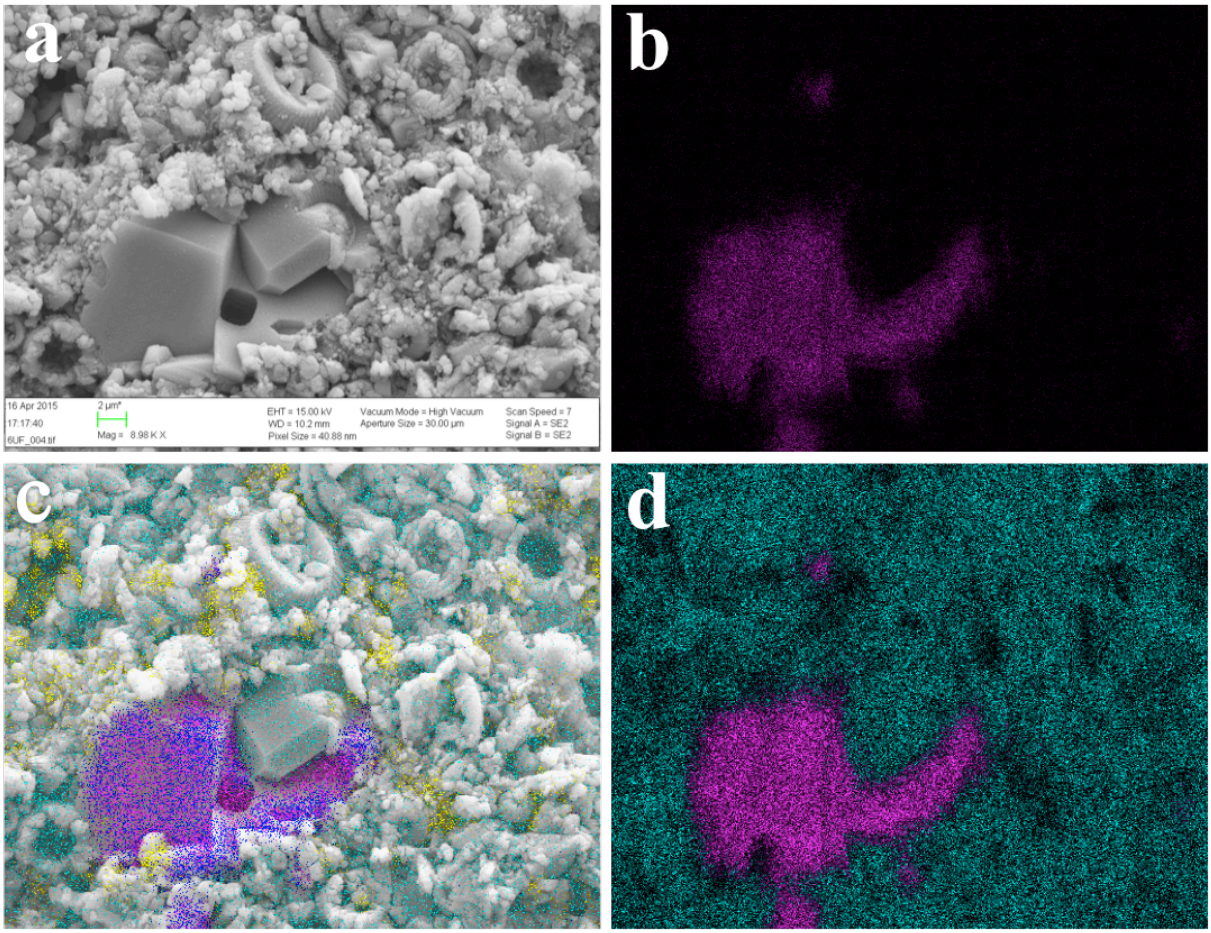

Figure14: Halite (salt) crystal and chemical composition maps; the resolution of the density maps increases the more times the image is scanned: (a) SE micrograph; (b) sodium density map, with sodium displayed in pink; (c) overlay of micrograph and salt (pink elephant) silica (yellow) and calcite (teal); (d) sodium (pink) and calcite (teal) density map; density maps have the same scale as the SE image

Sample 1UF (Figure 15a) is the youngest of the samples, and lies highest in the stratigraphy. Much like the other samples, it consists of coccolith matrix, but the grains are less compacted compared to the older 12UF. The most obvious difference however is more various and abundant minerals (Figure 15a, b, c, d, f). This is clearly seen in the BSED images, with the clay minerals seen as light grey, almost white (Figure 15b) distinguishable against the darker grey of the calcite grains. They occur in flakes of about 1 μm size, with curly edges, laths and hairy morphologies.

Apatite (Figure 15c) is the most common of the phosphate minerals and it is widely distributed as an accessory mineral in almost any type of rock as microscopic crystal. It can be white, green, or brown; it is brittle, soft, and without a good cleavage. The apatite crystals are hexagonal prisms, very often rounded at the ends (Dietrich and Skinner, 1979).

Calcispheres are common, seldom cemented, or filled with coccolith debris, and are sometimes deformed (Figure 15e). They are hollow, or often contain precipitated calcite crystals.

Another notable find is a detrital quartz grain, rounded, indicating transportation (Figure 15f).

Biotite (Figure 16) is a phyllosilicate belonging to the Mica Group, recognized by its brown to black color and perfect micaceous cleavage along the layered sheets. It forms in a large variety of geological environments and it is present in many igneous, sedimentary, and metamorphic rocks (Bonewitz, 2008).

Pyrite (Figure 17) is the most common of the sulfide minerals, and due to its metallic luster and brass-yellow color, it is often mistaken for gold. It is opaque and it has a rather high hardness for a sulfide (6 to 6.5). Because pyrite forms in anoxic conditions, it often replaces decayed or dissolved fossils (Dietrich and Skinner, 1979).

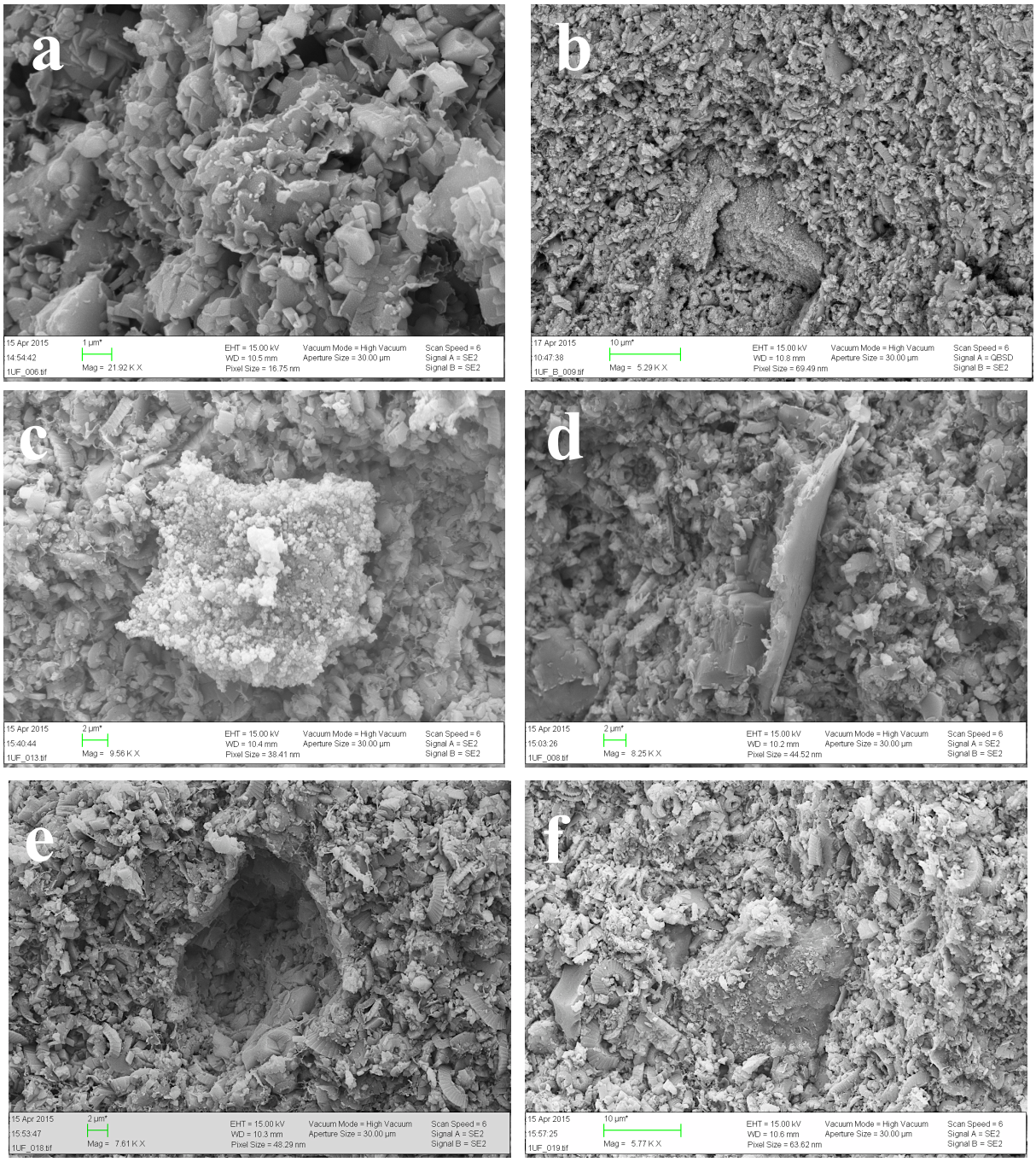

Figure 15: SEM micrographs of sample 1UF: (a) coccolith matrix and thin fibrous clay minerals; (b) BSE image showing the distribution of the calcite (darker shade of grey) and clay minerals (light grey, almost white thin fibers); (c) apatite crystal seen with the SE detector; (d) mica flake; (e) deformed calcisphere; (f) detrital quartz grain, rounded from transportation and weathered

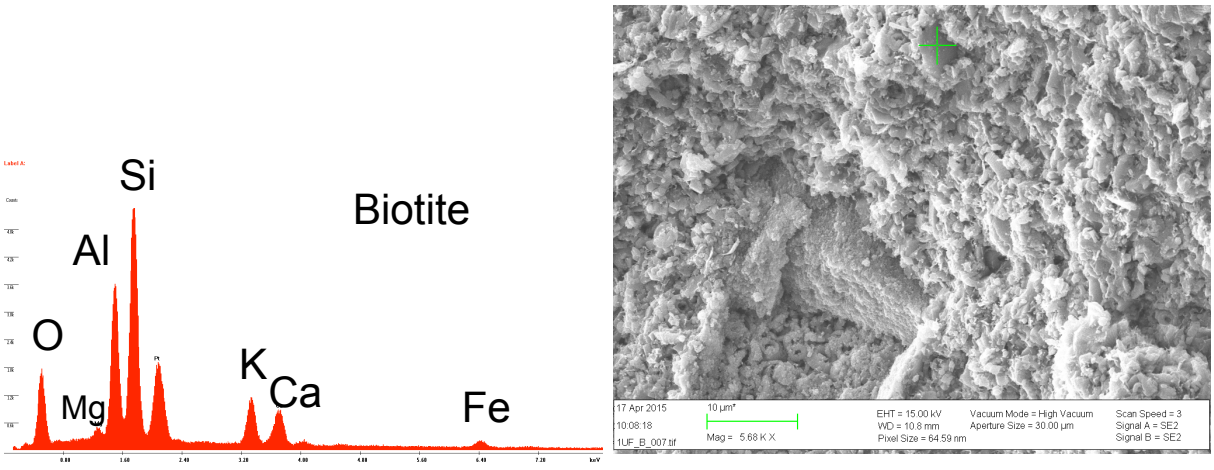

Figure 16: Left: EDS spectrum of biotite, with typical peaks of Si, Al, O, K and Fe; Right: SE micrograph with the measuring spot (green cross); Ca occurrence points to massive abundance of calcite also in the vicinity of biotite, which makes it often impossible to spot the chemcial composition of one non-carbonate mineral

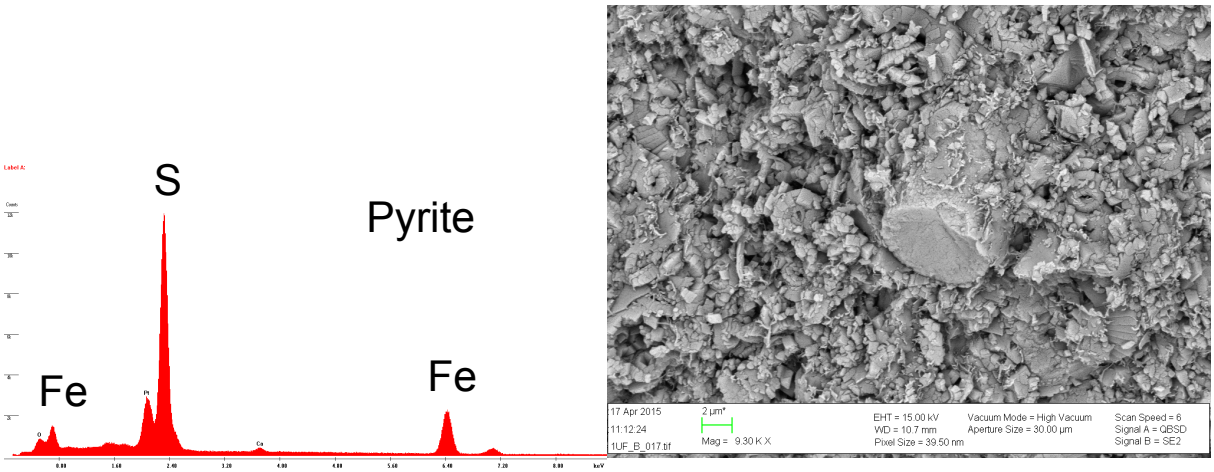

Figure 17: Left: EDS spectrum of pyrite, with a clear sulfur peak and primary and secondary iron peaks; note the Ca peak present here; Right: pyrite crystal in the center of the BSE image

5.2.2 Flooded chalk

Sample 11WF lies just above 12UF and it has similar features. Many of the calcispheres are deformed, broken, or filled with coccolith debris, or calcite crystals (Figure 18a). Calcite cement is common, at times filling calcispheres entirely (Figure 18b). Besides calcite, chalcopyrite is also present in this sample (Figure 18c, d). Chalcopyrite also belongs to the Sulfides Group; it has a similar appearance to pyrite, but differs in hardness (softer than pyrite). The chemical composition includes copper and calcium, besides sulfur and iron.

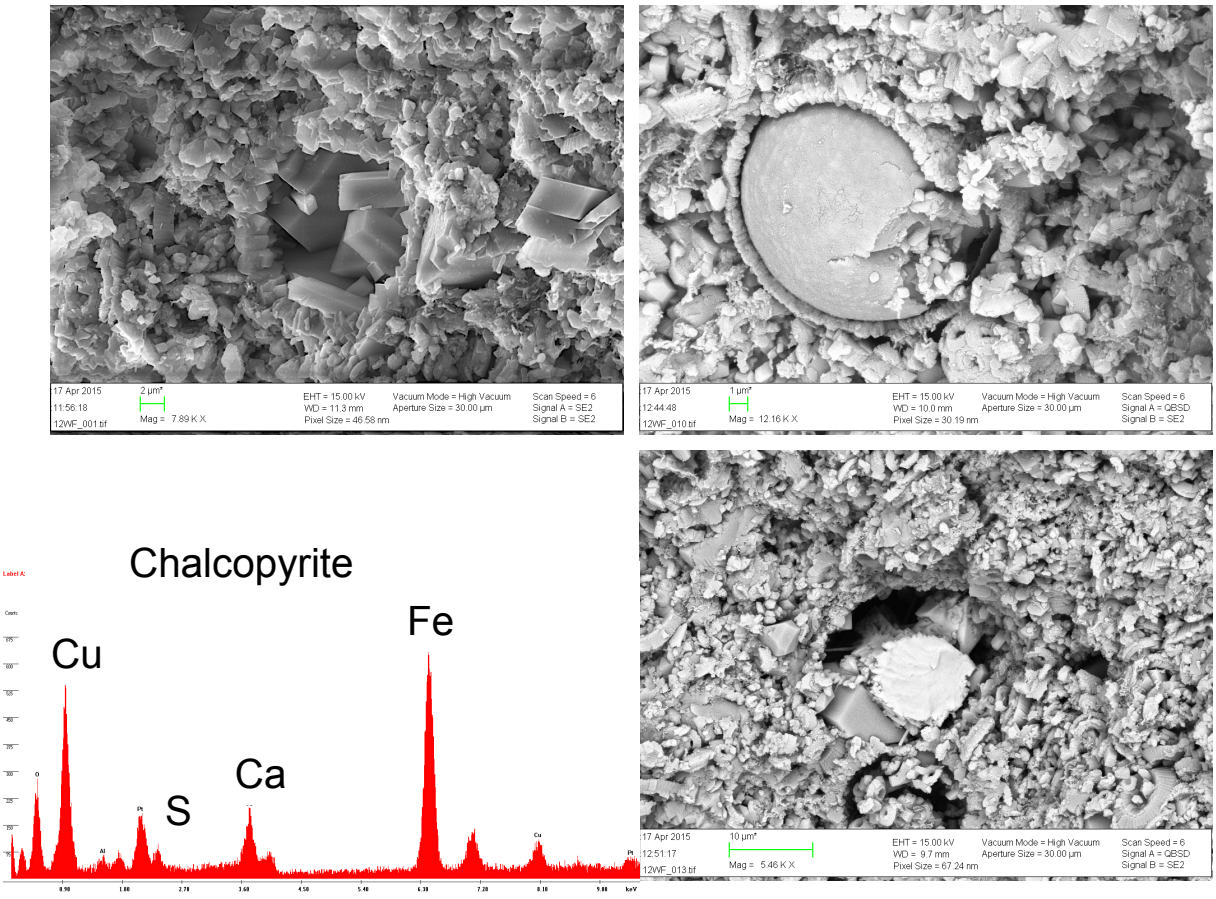

Figure 18: Sample 11WF: top left: calcipshere almost entirely filled with precipitated calcite crystals; top right: cemented calcisphere; bottom: EDS spectrum of chalcopyrite, with copper and calcium peaks besides sulfur and iron; bottom right: BSE image of the chalcopyrite in the center, reflected as almost white, compared to the calcite matrix

Further up in the stratigraphy, sample 9WF shows high homogeneity. The slightly lighter grey area in the center of the BSED image is calcite, the tone contrast indicating a local higher density (Figure 19).

The mineral composition maps reveal higher silicon abundance and both clay minerals and quartz are present. A multichamber foraminifer seen in the sample is cemented with calcite; the central chamber seems to be deformed, elongated and it appears in a lighter grey tone in the BSED image (Figure 19c, d). BSE images and EDS spectra reveal the presence of kaolinite, although in a small proportion (Figure 19e, f).

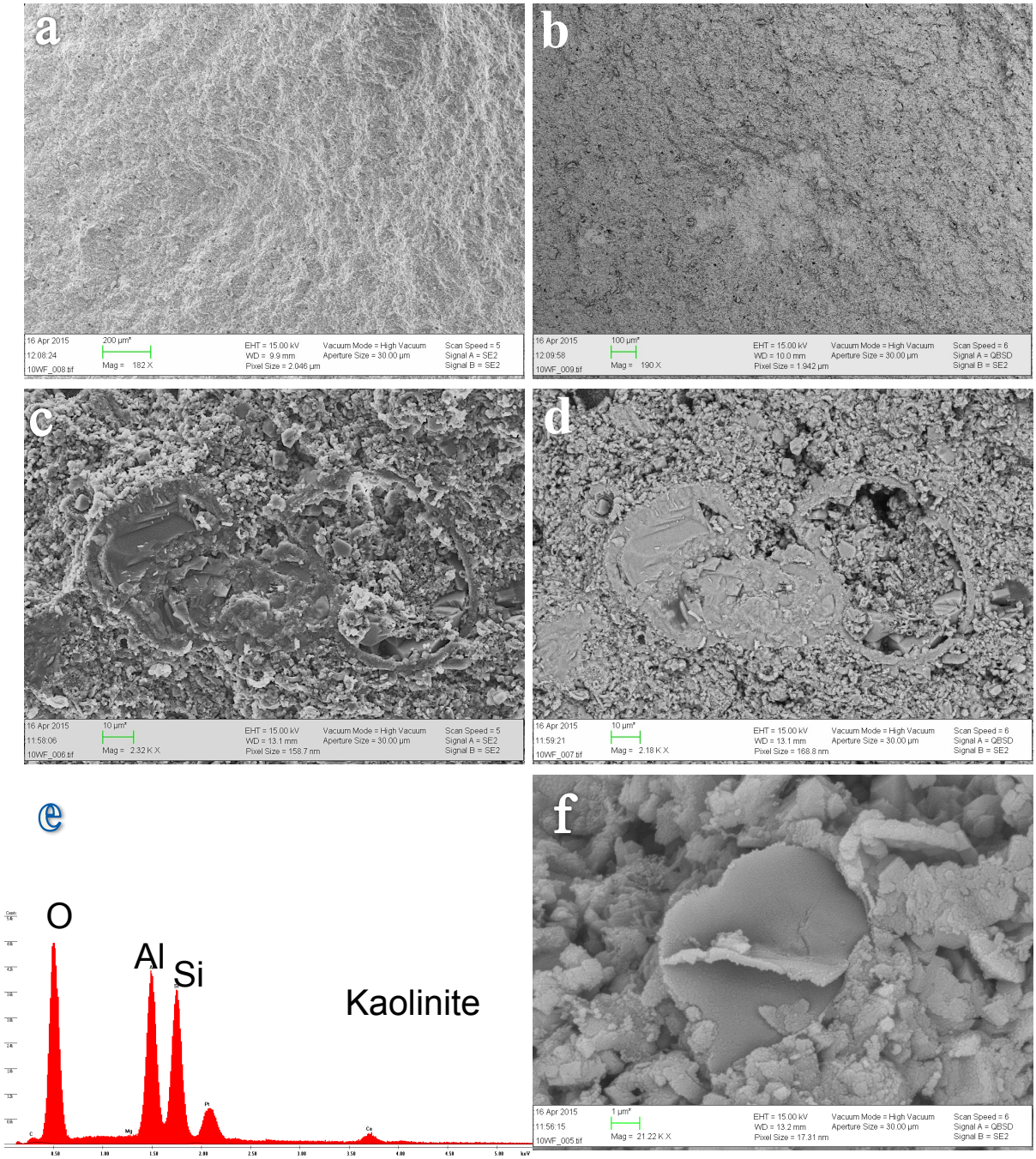

Figure 19: Micrographs of sample 9WF: (a) SE overview of the sample showing high textural and compositional homogeneity; (b) BSE image of calcite matrix with a more dense calcite area appearing as a compositional contrast; (c) multichambered foraminifer, two of the chambers entirely cemented with calcite; (d) BSE image of the foraminifer, revealing a denser cemented area and deformation of the chambers; (e) EDS spectrum of the kaolinite detected in the sample; note the presence of Ca peak; (f) BSE micrograph of the kaolinite grain

Sample 7WF contains, besides the coccolith matrix, calcispheres both hollow, and filled with coccolith fragments and precipitated calcite crystals (Figure 20a, b). Sponge spicules are also present; the siliceous skeleton is dissolved, being sometimes partially, or entirely replaced with calcite (Figure 20c, d). One notable occurrence is a rounded, weathered calcite grain, indicating transport and detrital origin (Figure 20e).

The sample surface is covered in ice, reducing the image accuracy. During sample preparation, the chalk fragment came in contact with liquid nitrogen. The higher temperature in the liquid nitrogen compared to the semi-solid state (slush) allows the water in the pores to crystalize before the sample is vitrified. However, this does not affect the BSED images, or the EDS analysis.

None of the five reservoir chalk fragments investigated with cryo-SEM showed any trace of hydrocarbons, although highly anticipated. Because the subsample size is very small, it could have eluded the oil saturated pores assumed by the optical petrography. Another reason could be the prolonged storage of the cores before and during processing in conditions that may have lead to evaporation of the hydrocarbons.

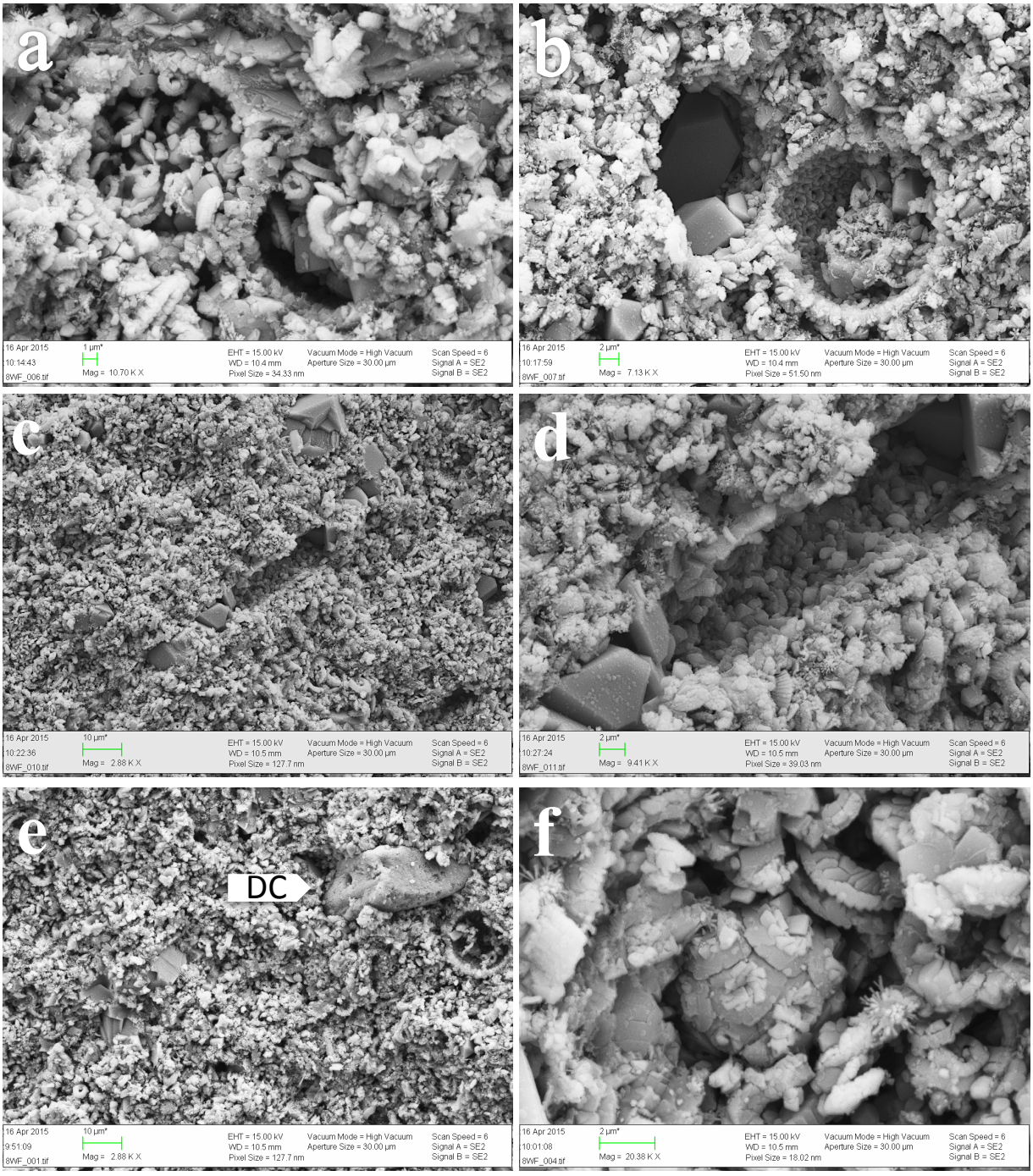

Figure 20: Micrographs of sample 8WF: (a) entire, or broken calcispheres, filled with coccolith debris; (b) calcisphere cavities filled with precipitated calcite crystals (left) or coccolith debris (right); (c) sponge spicule (monoaxon) partially filled with calcite crystals; (d) close up of the spicule, showing the cavity left after the siliceous skeleton was dissolved, creating large secondary pore space; (e) DC – detrital calcite showing distinct signs of weathering and transporation; (f) the ice layer on the sample reduces the image quality

5.3 XRD results

5.3.1 Whole-rock

Whole-rock x-ray diffraction scans show that the rocks are dominated by calcite, and quartz is present as an accessory mineral in all samples, representing less than 10% of the rock composition (Appendix C). None of the silica content is related to opal. Calcite and quartz have a high reflectance to the x-rays, and are therefore easily detectable. The peaks are a reflection of the mineral abundance (the higher the peaks, the more abundant mineral) and their positions in the spectrum reflect the different mineral phases.

The restricted mineral assemblage is consistent in all core samples, both unflooded and waterflooded. The variations in trace components are not very well seen in the whole-rock spectra.

5.3.2 Non-carbonate fraction

The most abundant mineral in the non-carbonate separates is quartz (80-90%) (Figure 21). Plagioclase and kaolinite are detected and represent a similar proportion, while illite occurs in smaller amounts. Traces of smectitic material can be seen in all samples, and potentially amphiboles. Chlorite can also be considered, but since its peaks positions are commonly overlapping those of kaolinite, a positive distinction between them cannot be made at this stage.

Although the resulting non-carbonate separate is naturally within the fine silt-clay size, it is important that the sample preparation avoids crystal orientation. Tabular, prismatic minerals like phyllosilicates tend to have a higher preferential dimension, which complicate the result interpretation. For the scope of clearly identifying the clay mineral suits, a different sample preparation routine is therefore required.

Sample 12UF, like all the other samples is most abundant in quartz. The carbonate content has not been entirely dissolved (similar to sample 2UF) and calcite peaks, representing

different phases of the mineral, can be detected. The kaolinite (or chlorite) proportion is small, but significant (5%), compared to the less evident smectite, illite, and plagioclase. One notable peak at position 28,97Å is interpreted as halite.

Sample 10WF shows the same quartz abundance, but the amount of illite and smectitic material is slightly higher than in sample 12UF. The peak representing the plagioclase is also more prominent.

Sample 9WF differs from 10WF in that the traces of smectitic minerals (smectite, or mixed layers of illite and smectite, or chlorite and smectite) are somewhat more defined. Similar mineral proportions are seen in sample 2UF.

Sample 1UF contains the largest variety of non-carbonate minerals compared to the rest of the samples. Quartz is still the most abundant, but the peaks for smectite, chlorite and/or kaolinite, plagioclase and phyllosilicate minerals are more distinct than in other samples (the peaks are narrower and register more counts).

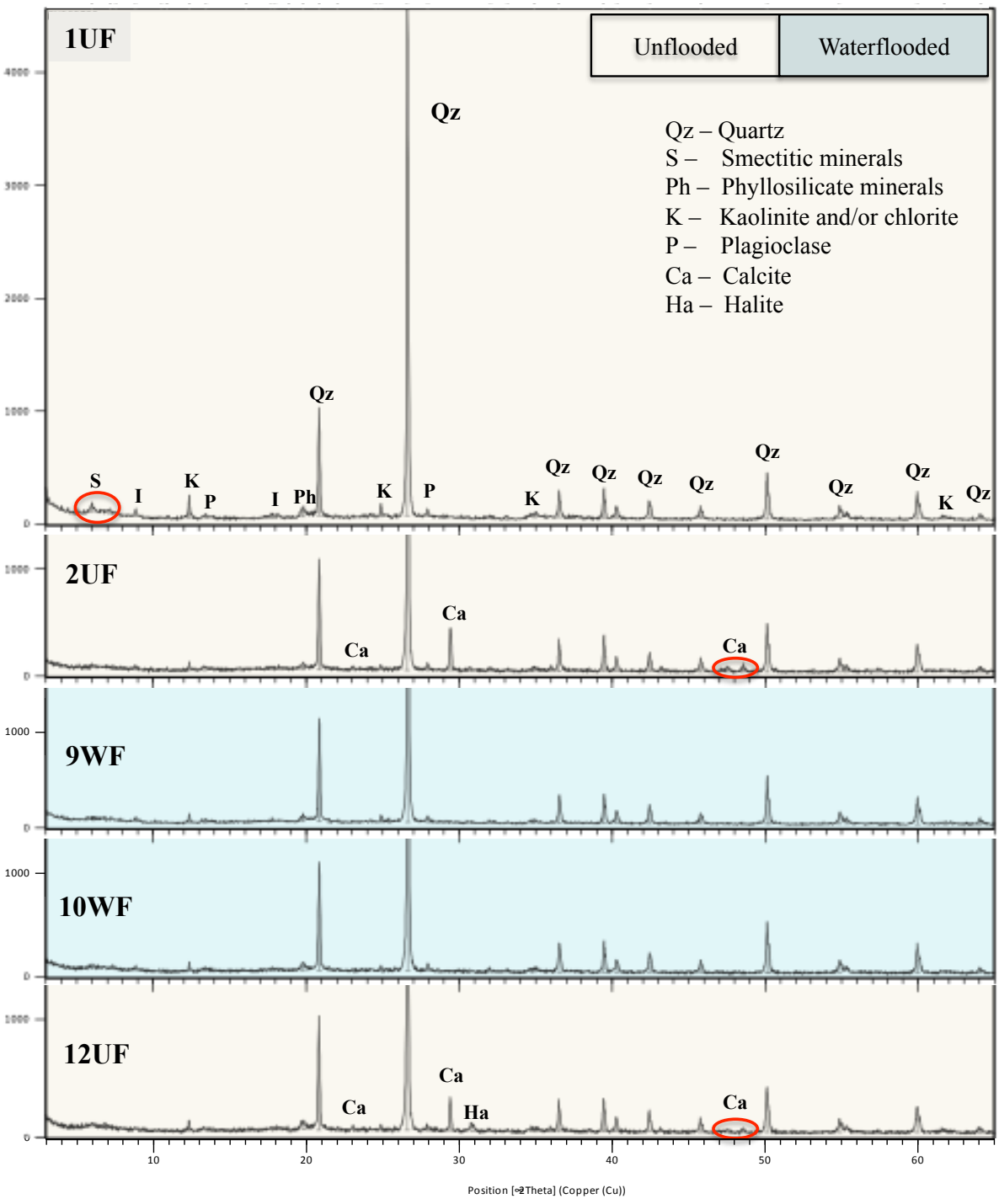

Figure 21: XRD spectra of non-carbonate content from 5 different cores, both flooded and unflooded showing mineral diffraction angles versus counts; all samples have a similar composition, regardless of their flooding status. Red ovals mark a group of peaks representing the same mineral

5.4 Isotope Geochemistry Results

The standard deviation of the powdered coral laboratory standard (COR1D, $\delta^{13}C_{PDB}$ = -0.648, $\delta^{18}O_{PDB}$ = -4.920) run as a sample on the same days as the study samples was ± 0.04‰ for $\delta^{13}C$ and ± 0.06‰ for $\delta^{18}O$.

5.4.1 Carbon isotopes

The $\delta^{13}C$ values range between 0,70 and 1,75‰ (open folded page, Appendix C). Most of the negative excursions seen in the curve represent the probes taken from cut surfaces, either lab cuts, or core surfaces. The carbon isotopic composition sampled from fresh surfaces is however less variable, between 0,91‰ and 1,75‰ and the majority plots within the analytical precision, marked on the graph by the shaded rectangle. One core sample stands out, 7WF, with all the measured values representing a negative excursion on the curve. One other value, from core 5UF, plots clearly outside of the error range.

5.4.2 Oxygen isotopes

Similarly to the carbon isotopes, the $\delta^{18}O$ values from the first well are consistent, and after removing the anomalous values from the lab cuts and core surfaces, they range between -4.59‰ and -3.77 ‰. The majority is undisturbed, with the exception of core 7WF and 5UF, which represent a negative shift on the curve (folded page, Appendix C).

The oxygen isotopic values indicate temperatures between 28°C and 32°C.

5.5 Geochemistry results

5.5.1 Whole rock geochemistry

The major element geochemistry of the whole rock analysis shows, besides calcium oxide (CaO) as the highest proportion of major elements (between 46.2 – 49.7%) also a high content of silica (SiO_2) in all the subsamples, ranging between 6.81 – 10.81%.

Aluminum oxide (Al_2O_3) is present in a much smaller proportion, averaging at 0,6%. The magnesium oxide (MgO) and iron oxide (Fe_2O_3) content is similar, at an average of 0,2%.

The top two cores, 1UF and 2UF count for most of the extreme values. Core 1UF has the lowest CaO content and consequently highest weight percent of SiO_2, MgO, K_2O, Al_2O_3, or Fe_2O_3. The rest of the cores have a very similar major and minor element composition, with very little variation between values, although they seem to slightly increase with depth, while the loss of ignition (LOI) values decrease with depth.

The concentration of strontium is high for a carbonate, ranging between 1097-1268 ppm, while Rb and Zr record values of 3, respectively 4 ppm, representing more than 2% of the typical values for the Post Archaean Australian Shale (PAAS).

The Rare Earth Elements (REE) and yttrium concentrations are normalized to the PAAS values, and reflect a general depletion of the REE by an average factor of 6. The enrichment in La, depletion of Ce and a positive Y anomaly are a typical signature of open marine seawater composition (Figure 22). Sample 1UF stands out with overall higher normalized REE values (e.i., closer to PAAS composition).

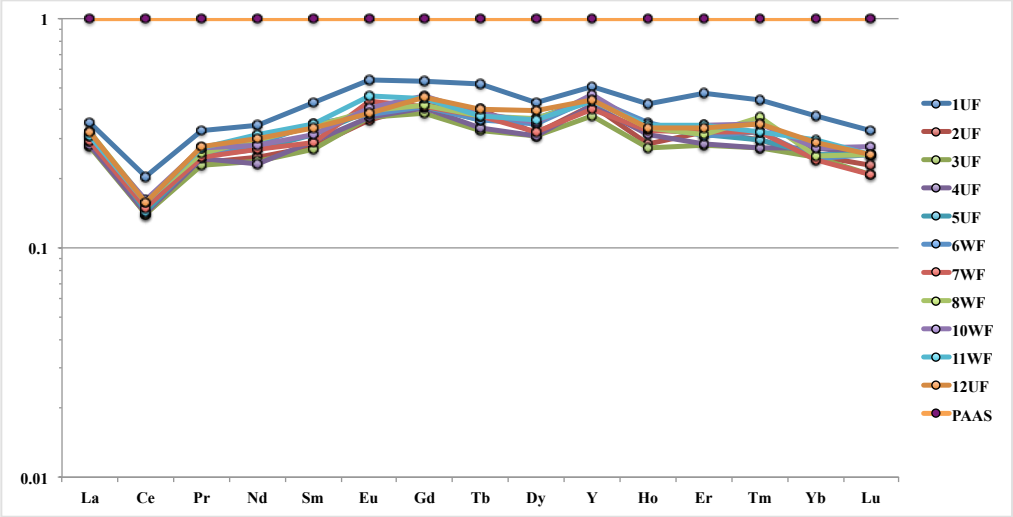

Figure 22: Shale normalized Rare Earth Element chemistry (REE/REE_{PAAS}) with REE patterns of the reservoir chalk, showing an increase in the MREE (middle REE) and depletion of the HREE (heavy REE)

The Y and Ho concentrations have a positive linear correlation, also typical for marine environment. The Y/Ho ratios average at 36 (Figure 23), a fractionation ratio that is lower than what would be expected for seawater. The same ratio calculated on the non-carbonate fraction composition has an average of 32.

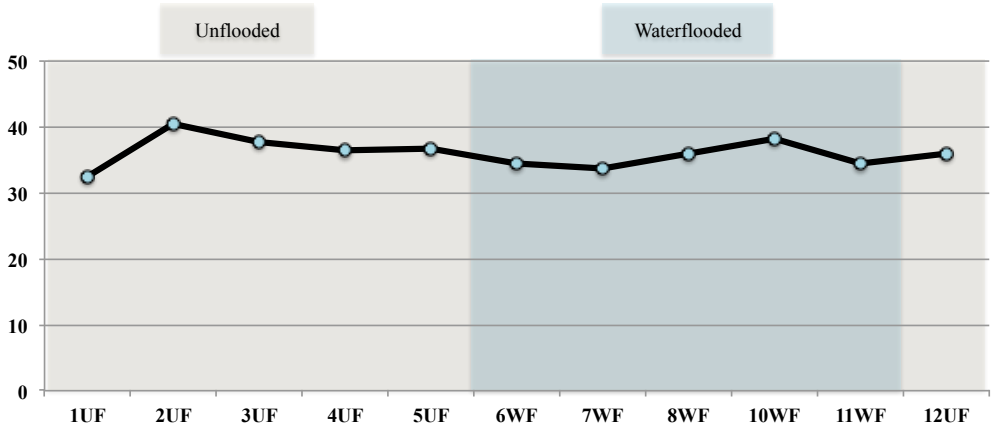

Figure 23: Homogeneous Y/Ho ratios in the whole-rock composition from bottom of stratigraphy (left) to the top of the sampled section (right); note the similarity between the unflooded and waterflooded samples

5.5.2 Non-carbonate fraction geochemistry

The non-carbonate content is chemically represented mostly by silica (67% - 75%). The highest amount of silica and aluminum oxide is found in sample 1UF, while the other samples have a more similar composition, with an average of 5% aluminum oxide. The unflooded

samples 2 and 6 have still a significant CaO content and LOI relative to the rest of the samples. Other major elements are represented in a small proportion.

The shale normalized REE patterns show higher REE abundances than the whole-rock analyses but still a significant Ce anomaly (Appendix C) and increase of MREE followed by a depletion of the HREE (Figure 24).

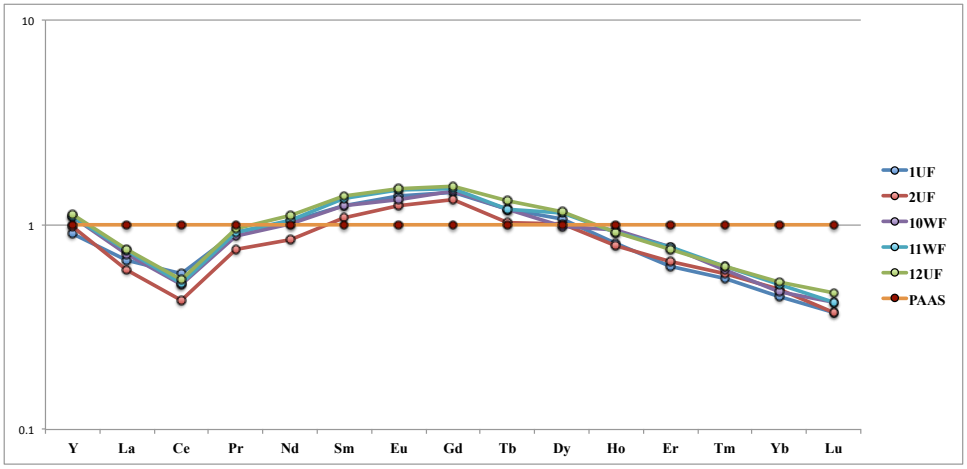

Figure 24: REE+Y pattern seen in the non-carbonate fraction

A full overview of element concentrations is listed in appendix C.

6 DISCUSSION

Sediment composition and physical properties

The optical petrography and SEM imaging revealed a sediment composition typical for Upper Cretaceous chalks, consisting of micritic carbonate matrix, microfossils and diverse authigenic and detrital minerals. The deposition of the coccoliths, the space between the whole and disintegrated calcite platelets, are the primary source of porosity that makes this a good reservoir rock. The preserved calcite skeletons of calcispheres and foraminifers are efficiently enhancing the chalk porosity, as well as the void left after the dissolution of the sponge spicules. Another factor contributing to the high porosity and good permeability is the fracturing of the chalk, as veins and interconnected crack networks. Other studies on the mechanical and chemical effects on porosity and permeability (e.g., grain coating, pressure

conditions) can contribute to a more thorough property description, but are not a part of this project.

Diagenetic processes reduce porosity, as fractures, spicules, and microfossils are often entirely or partially filled by in situ precipitated calcite, or calcite cement; the older samples that are deeper buried show microfossils that are often deformed, or have collapsed walls, and filled with ultra fine matrix material.

Another factor that weakens the reservoir quality and proves to be a challenge for the hydrocarbon recovery is the high clay mineral content seen especially in the upper part of the stratigraphy.

Isotopic composition

Previous studies on primary carbon isotopes typical for Cretaceous suggest a stable trend, with little variation in the $\delta^{13}C_{PDB}$ values for the Upper Cretaceous stages, averaging at +2‰ $\delta^{13}C_{PDB}$ (Appendix C, Gradstein et al., 2012). The values of the carbon isotope ratio from the reservoir chalk are somewhat lower, indicating enrichment of the organic carbon, thus higher ^{12}C values compared to the global trend.

Similarly, the oxygen isotopes are more negative compared to the typical isotopic record of the Upper Cretaceous, and consequently warmer paleowater average temperatures.

The range of the carbon isotope values is very narrow, and it is consistent to the expected values of unaltered chalk, indicating mainly a primary carbon source. However, the negative shift suggests that the overall isotopic composition does not entirely reflect the water in which the minerals have been precipitated (Figure 25).

The diagnoses of the disturbing factors can rule out hydrocarbons, as both the oxygen and carbon isotope ratios throughout the stratigraphic profile are rather consistent and show parallel anomalies. The sporadic negative excursions registered in samples 7WF and 5UF

suggest an external carbon source with an isolated effect, possibly a secondary input material. Also, the positive covariation between $\delta^{13}C$ and the $\delta^{18}O$ from these two particular cores can be an indication of mixing of seawater and circulating fluid. The depletion of ^{18}O and enrichment in ^{12}C of meteoric water, or other non-marine fluid, like intraformational water, relative to the seawater causes the isotopic ratios to change synchronously (Rollinson, 1993).

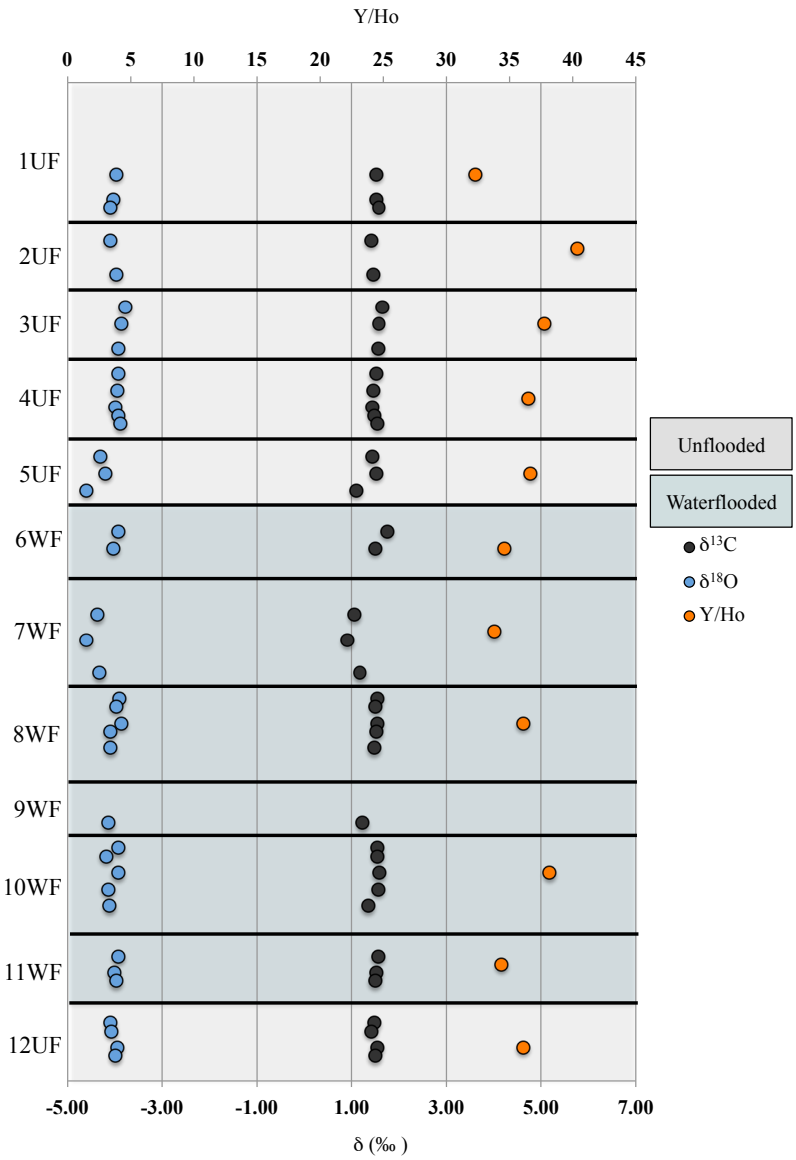

Figure 25: Combined stable isotope curves and Y/Ho ratios from the sampled section showing little variations throughout the profile and clear negative excursions of the isotopic ratios and lower Y/Ho from sample 7WF

Clastic input versus secondary fluid

The overall sum of REE for clean carbonates should be very low and higher values, like in this case, are an indication of terrestrial input and/or secondary fluid flow (Frimmel, 2009). Clastic input can be undoubtedly seen in the SEM, XRD and the whole-rock geochemistry.

Kaolinite as an example is rarely authigenic, often occurs as secondary deposits formed by hydrothermal alteration, and is an indicator of deltaic, lagoonal, or other non-marine environment (Dietrich and Skinner, 1979). Besides kaolinite, the XRD, SE, BSE and EDS analyses showed a large variety of clay minerals and detrital grains.

The characteristics of a "dirty chalk" or marly chalk are supported by the high silica content (an average of 9%, compared to lower than 2% expected for pure chalk). The SEM micrographs and EDS scan show both clay minerals and detrital quartz as the source of silica; also contributing to the silicon supply is the dissolving of the sponge spicules, highly abundant in some of the cores (Madsen et al., 2010).

The clastic provenance of the clay particles is also recorded in the high concentrations of Rb and Zr, in the whole-rock samples, with values above 2% of the PAAS, which suggest several geochemical proxies have a clastic origin. The geochemistry of the non-carbonate separates points to a typical unrecycled Upper Continental Crust composition (UCC, Taylor and McLennan, 1985) when plotting Zr/Sc versus Th/Sc, and most of the values are comparable to those of the UCC. The flat shape of the REE patterns in the clay fraction and Dy/Yb ratios above 1.8 (Appendix C) also reflect a non-marine environment (Shields and Webb, 2004).

However, the clastic sediment is not abundant enough to cause all the alterations seen in the geochemistry of the chalk, which supports the assumption of another contaminant, most likely a secondary fluid.

Marine vs meteoric water

In respects to identifying the fluid in which minerals have been precipitated, Sr, Y and REE are useful indicators. Analyses on the chemical composition of the ancient seawater show that the distribution of the REE does not suffer substantial changes compared to the present-day seawater values (Shields and Webb, 2004) and should retain the characteristics of the original fluid environment.

In this case, the REE and Y pattern follows the typical open marine seawater signature, but at the same time the overall depletion is less than what is expected for (pure) chalk deposits.

Studies on the Y and Ho behaviors suggest that their relative abundance can be a useful tool in distinguishing between marine and non-marine deposits. The two elements resemble closely, but their differences result in a strong fractionation between the two, by a factor of 0.5 (i.e., Ho is removed two times faster than Y in seawater). Because fractionation is minimally affected by weathering, or transportation, the main influence on the Y and Ho relative abundance is the ambient fluid. The fractionation mechanisms lead to much higher Y/Ho ratios in seawater (above 90) compared to river waters, which are close to the chondritic and shale ratios (Frimmel, 2009; Nozaki et al., 1997).

The positive linear correlation between the abundance of the two elements in the geochemistry results indicates that the fractionation took place in a marine environment. However, the low Y/Ho ratios (ca 36) seen in the North Sea reservoir chalk are much below what is typical for seawater, and therefore reflect the presence of another fluid, assumingly fresh, meteoric water, or intraformational water stored in rock successions.

New growth and secondary cement have been observed in the rocks via SEM and optical microscopy, but neither dolomite nor Mg-rich calcite could be detected. This suggests that the new growth is rather due to circulating intraformational water, which dissolved the original

mineralogy and allowed the precipitation of massive carbonate, than to the excessive fluid flow form meteoric sources.

The estimation of the diagenetic grade is not possible at this stage. The clay minerals are most readily adjusted to the changes in the chemical conditions during burial, and this is seen in the change in mineral phase. XRD analyses can identify such diagenetic changes, by considering the change in the mineral assemblage (e.g., from smectite to illite downwards). Further down in the stratigraphy, a change from illite to muscovite can be interpreted as low-grade metamorphism. Hence, future studies on separated clays from the non-carbonate fraction can determine a secured value.

Unflooded versus waterflooded chalk

The variations seen in the optical microscopy, SEM, XRD spectra, C-O isotope curves, and REE trends are not related to the flooding status of the core plugs. This indicates that either the post-depositional geological overprint by diagenetic processes, or a strong intraformational fluid reset the data, and that the water flooding by EOR means did not affect the chalk as such that it could be recorded by the here used methodology.

8 CONCLUSION

The here presented research study is based on approximately 1m of reservoir chalk of Upper Cretaceous age, from the North Sea, ranging over 47m of vertical stratigraphy. The samples are core plugs from horizons that are either unflooded, or waterflooded.

A thorough reservoir chalk characterization is an essential part of the EOR research within the National Improved Oil Recovery Center of Norway (NIOR), led by the University of Stavanger, in cooperation with other research institutes and industry partners.

Methods like optical petrography, SEM, XRD, stable isotope geochemistry, and rock geochemistry were employed in order to gain insight into the uniqueness of the North Sea reservoir chalk composition, and describe its petrography, physical properties, the mineral assemblage, and geochemical print.

Mineralogically, the chalk consists mainly of calcite; the silica is stored mostly in quartz and it represents a smaller, but significant proportion of the mineral makeup of the chalk (9%). Corroborated results from XRD, SEM and geochemistry indicate the presence of other non-carbonate mineral phases like illite, smectite, kaolinite, which confirms a significant clastic input.

The carbon isotopes seem to reflect the primary carbon source, although the $\delta^{13}C$ values are slightly lower than the global trend. The oxygen isotopes are more sensitive to disturbing factors, and this is more clearly seen in the $\delta^{18}O$ curve for the reservoir chalk. The positive correlation between the $\delta^{13}C$ and $\delta^{18}O$ anomalies can be an indication of a secondary fluid. Alterations associated with secondary fluid flow can also be seen in the REE patterns.

Since the flooding status of the cores does not seem to control the changes in the chemical composition of the chalk, the alterations are most likely a result of diagenesis, which induced the fluid flow responsible for the new growth. Whether the secondary fluid is fresh, meteoric, hydrothermal, or intraformational stored water is not clear so far.

Future work

It is clear that the methods employed in this study provided valuable information about the petrography and the mineralogy of the reservoir chalk in the North Sea area. However, refined measurements and a wider study area would be beneficial for a more detailed rock characterization. Thus, new carbon and oxygen isotope geochemistry analysis on samples avoiding drilled surfaces should provide a more accurate and representative isotopic curve. Also, analyses on core samples from several other wells can enhance the understanding of the North Sea reservoir chalk and provide a more broad description, at a larger scale. This is fully possible, and the measurements can continue beyond the time allocated to this project, on several meters of available core samples from four other wells in the area, and not the least, with new laboratory equipment that allows key measurements at the University of Stavanger, reducing processing time and costs.

Besides the methods used in this study, there are numerous other analyses that can be carried out to strengthen, improve and widen the reservoir chalk characterization: clay mineral separation and determination of the exact diagenetic grade, Raman spectroscopy, radiogenic isotope analyses, specific surface measurements on both rock pulp and clay fraction, mineral liberation analysis, and corroboration with log data provided by the operator company.

Another recommendation for future work could be taking a more meticulous approach to the rock-fluid interaction in the North Sea basin. This approach could identify the original pore fluid and clarify the timing of the hydrocarbon migration into the reservoir and the effects that it had on the chalk´s chemical composition.

The results and data interpretation in this study forms a solid starting point to a better understanding of the reservoir chalk in the North Sea basin, and establishes a base for comparison with onshore chalk in the attempt of finding the best equivalent for EOR purposes.

9 REFERENCES

Bjørlykke, K., and P. Avseth, 2010, Petroleum geoscience: from sedimentary environments to rock physics: Heidelberg, Springer, p. 470-480.

Bonewitz, R. L., 2008, Rock and gem: The definitive guide to rocks, minerals, gems and fossils: London, UK: Dorling Kindersley Limited, p. 55, 262.

Dietrich, R.V., and Skinner, B.J., 1979, Rocks and rock minerals: New York, John Wiley & Sons, p. 75, 83.

Emery, D., and A. Robinson, 1993, Inorganic geochemistry; applications to petroleum geology: London, United Kingdom: Blackwell Scientific Publications, p. 32-100.

Flügel, E., 2004, Microfacies of carbonate rocks: analysis, interpretation and application: Berlin, Heidelberg, Springer, p. 453-457, 491.

Frimmel, H. E., 2009, Trace element distribution in Neoproterozoic carbonates as palaeoenvironmental indicator: Chemical Geology, v. 258, p. 338-353.

Gharbi, R. B. C., 2000, An expert system for selecting and designing EOR processes: Journal of Petroleum Science and Engineering, v. 27, p. 33-47.

Goldstein, J. I., 1981, Scanning electron microscopy and X-ray microanalysis : a text for biologists, materials scientists, and geologists: New York, Plenum Press, p. 53-122.

Gradstein, F. M., J. G. Ogg, M. D. Schmitz, and G. M. Ogg, 2012, The geologic time scale 2012: Amsterdam, Elsevier Science & Technology, p. 200-216.

Hjuler, M. L., and I. L. Fabricius, 2009, Engineering properties of chalk related to diagenetic variations of Upper Cretaceous onshore and offshore chalk in the North Sea area: Journal of Petroleum Science and Engineering, v. 68, p. 151-170.

Kennedy, W. J., 1985, Sedimentology of the Late Cretaceous and Early Paleocene Chalk Group, North Sea Central Graben: North Sea Chalk Symposium May 1985, v. 1: S.l., s.n., p. 1-35.

MacKenzie, W. S., and A. E. Adams, 1994, A colour atlas of rocks and minerals in thin section: Rocks and minerals in thin section: London, Manson Publ., p. 9-28.

Madsen, H. B., L. Stemmerik, and F. Surlyk, 2010, Diagenesis of silica-rich mound-bedded chalk, the Coniacian Arnager Limestone, Denmark: Sedimentary Geology, v. 223, p. 51-60.

Misra, K. C., 2012, Introduction to geochemistry : principles and applications: Chichester, Wiley-Blackwell, p. 253-260.

Mortimore, R. N., 2014, Logging the chalk: Dunbeath, Whittles Publishing, p. 10.

Murphy, D. B., and M. W. Davidson, 2013, Fundamentals of Light Microscopy and Electronic Imaging, Hoboken, N.J, Wiley-Blackwell, p. 135-144, 150-171.

Norwegian Petroleum Directorate, 2014, Fact pages: http://factpages.npd.no/factpages/Default.aspx?culture=en (accessed 2014)

Nozaki, Y., J. Zhang, and H. Amakawa, 1997, The fractionation between Y and Ho in the marine environment: Earth and Planetary Science Letters, v. 148, p. 329-340.

Ramberg, I. B., A. Solli, Ø. Nordgulen, R. Binns, P. Grogan, and f. Norsk geologisk, 2008, The Making of a land: geology of Norway: Landet blir til: Trondheim, The Norwegian Geological Association, p.232-442.

Rollinson, H. R., 1993, Using geochemical data : evaluation, presentation, interpretation: Longman geochemistry series: Harlow, Longman, p. 266-302.

Shields, G. A., and Webb, G. R., 2004, Has the REE composition of seawater changed over geological time?: Chemical Geology, Vol. 204, No. 1-2, p. 103-107.

Taylor, S.R. and S.M. McLennan, 1985, The Composition and Evolution of the Continental-Crust - Rare-Earth Element Evidence from Sedimentary-Rocks: Philosophical Transactions of the Royal Society of London, v. 301, p. 381-399.
Van Holde, K. E., W. C. Johnson, and P. S. Ho, 2006, Principles of physical biochemistry: Upper Saddle River, N.J, Pearson/Prentice Hall, p. 242-310.

10 APPENDICES

10.1 Appendix A - Background

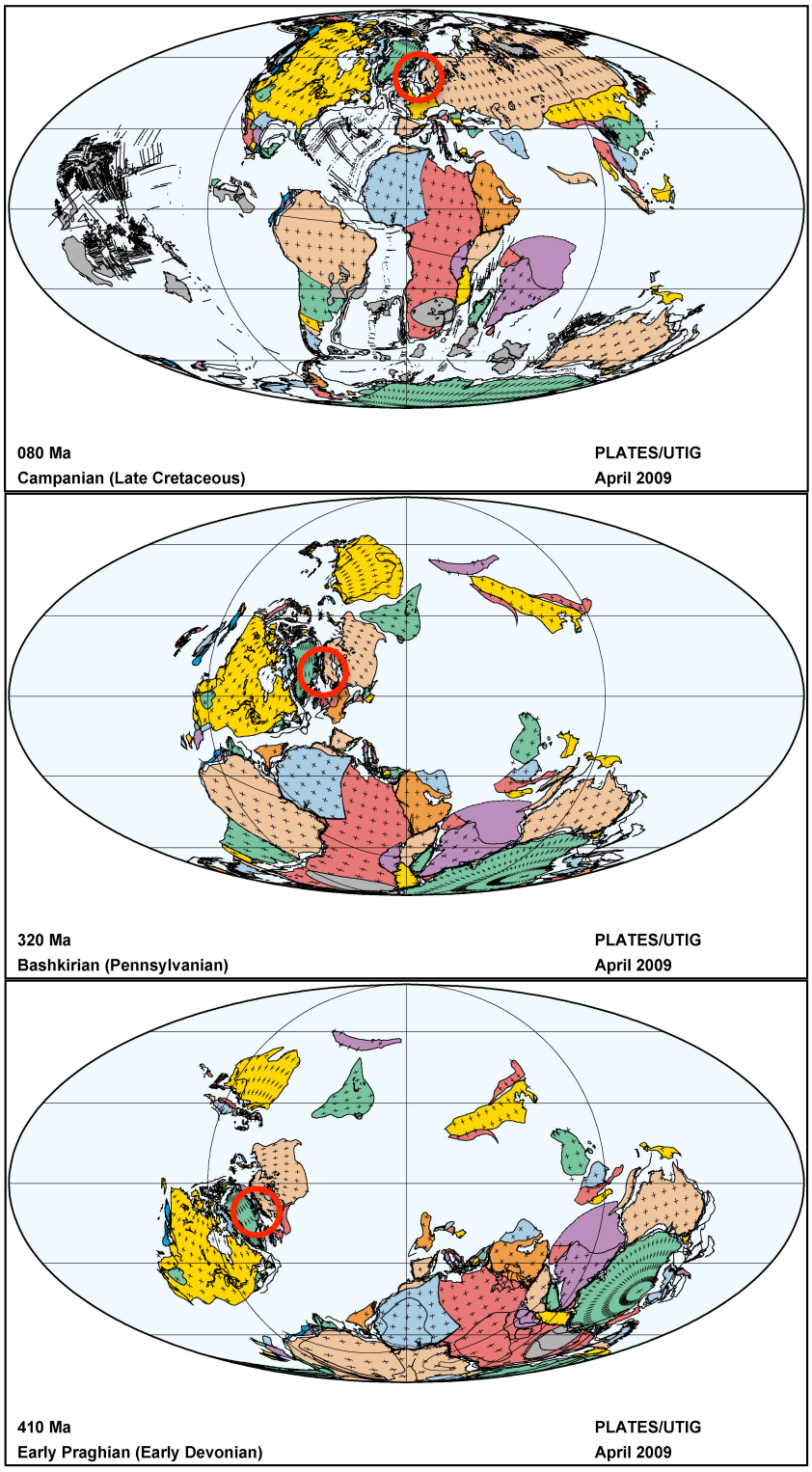

Figure 1: Tectonic evolution of the North Sea Basin, from the Atlas of Plates Reconstructions, 2009

LITHOSTRATIGRAPHIC CHART
NORWEGIAN NORTH SEA

NPD

2014

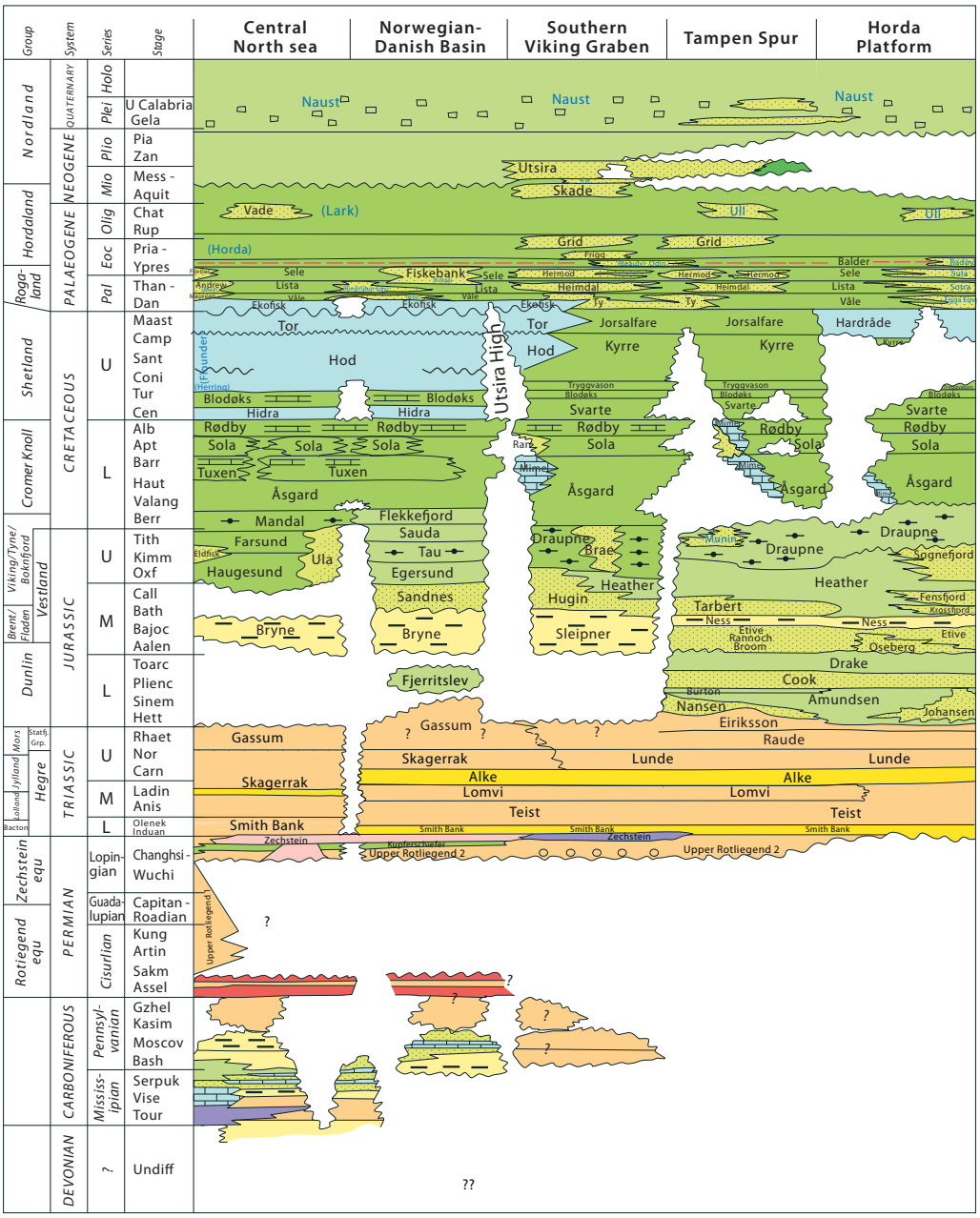

- Uplifted/eroded area
- Clastic continental deposits, mainly sandstone
- Clastic continental deposits, mainly shale and siltstone
- Salt (halite)
- Chalk
- Limestones, undifferentiated
- Volcanic deposits

(Informal names) - Formation names from UK or Danish sector
Informal names
Formal names

- Marginal evaporite deposits, sabkha
- Coastal, deltaic and flood-plain deposits
- Shallow-marine deposits, mainly sandstone
- Marine deposits, mainly shale
- Deep-marine deposits, mainly shale
- Shallow-marine deposits, glauconitic
- Calcareous shales, limestone and marl stringers
- Ice rafted detritus (IRD)
- Coal
- Volcanic tuff
- Source rock
- Conglomerate

OD 1409001

10.2 Appendix B – Samples and Sample preparation

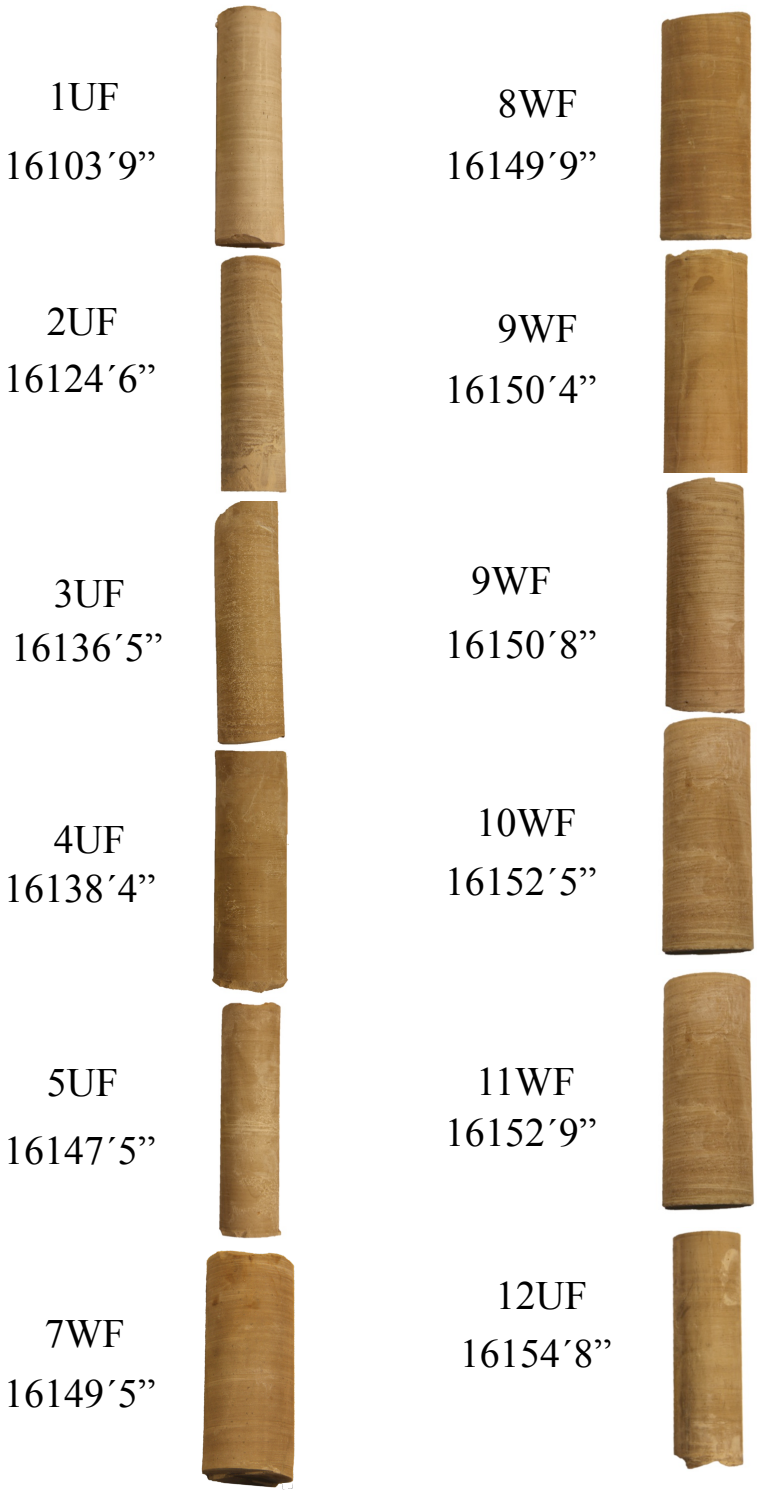

Figure 1: The core samples used for this research; each core plug has a 4 inch diameter; the depths are expressed in imperial units

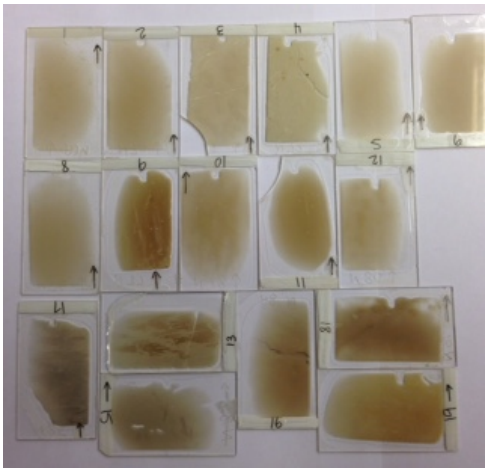

Figure 2: Thin sections

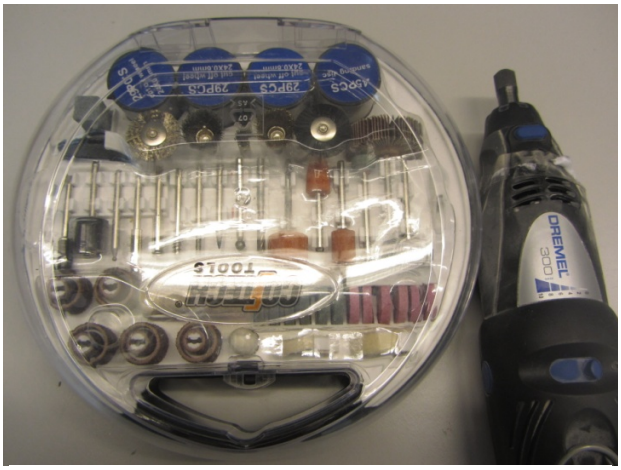

Figure 3: Dremmel and drill heads used for extracting the fine powder for mass spectroscopy

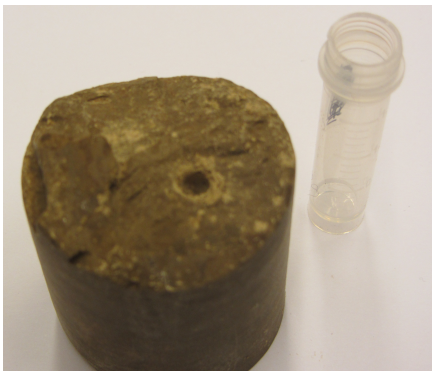

Figure 4: Drill spot on a fresh core surface and plastic container for the subsample

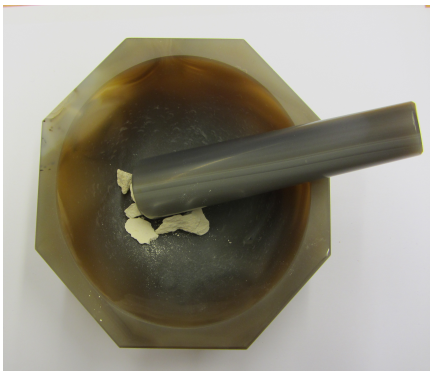

Figure 5: Agate beaker used for hand-milling the chalk for XRD analysis on whole-rock pulp

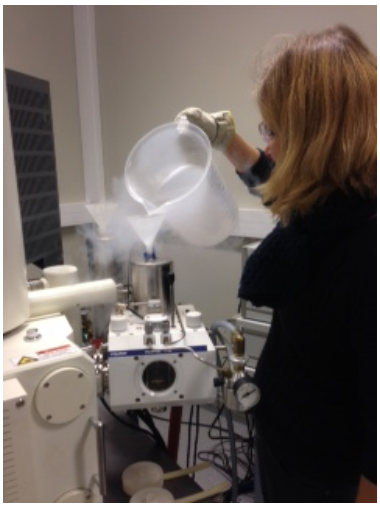

Figure 6: Cryo-SEM; regularly refilling the dewars with liquid nitrogen

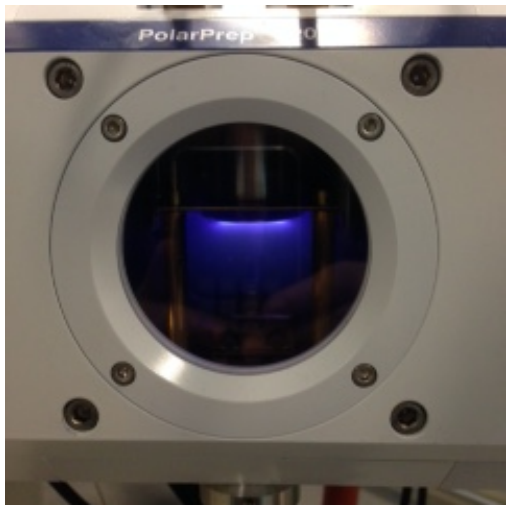

Figure 7: Platinum coating of the samples for cryo-SEM

10.3 Appendix C - Results

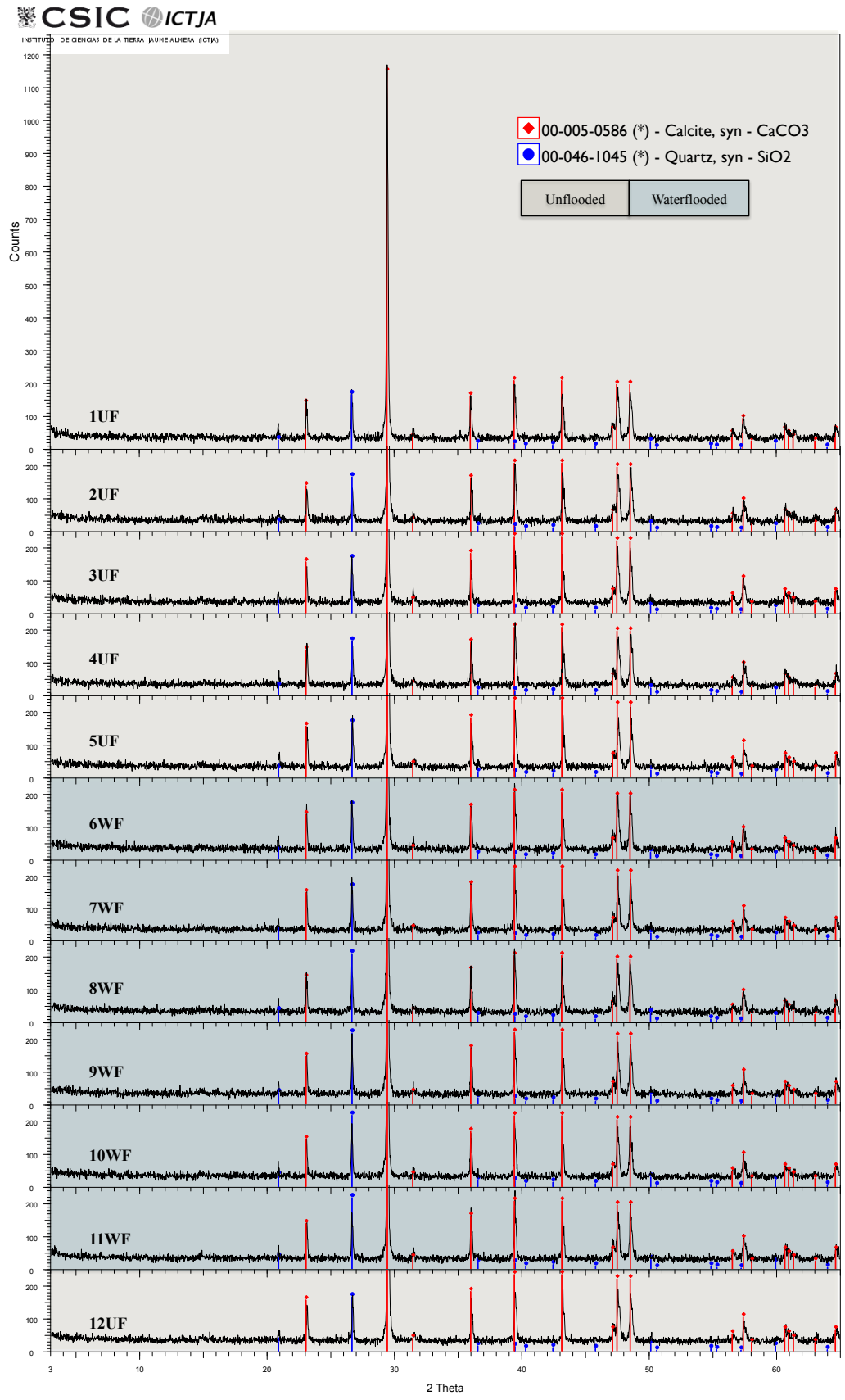

Figure 1: Whole-rock XRD analysis

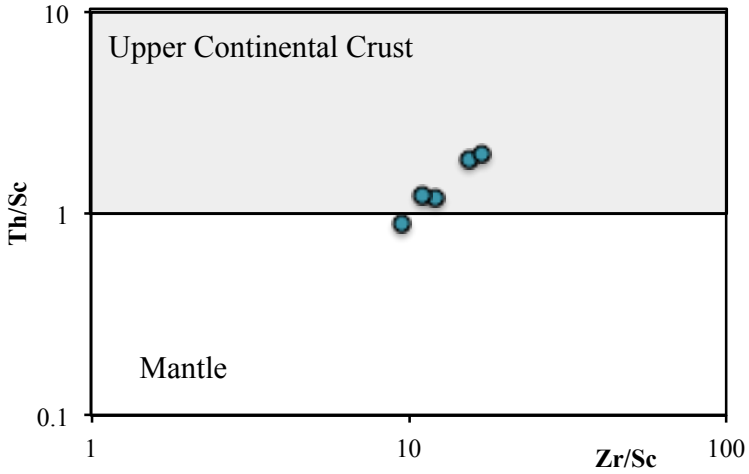

Figure 2: Provenance diagram showing Zr/Sc versus Th/Sc ratios from the non-carbonate fraction are mostly consistent with typical UCC values (after McLennan et al., 1990)

Figure 3: Shale normalized Dy/Yb ratios of the non-carbonates indicating secondary features that are unrepresentative of seawater

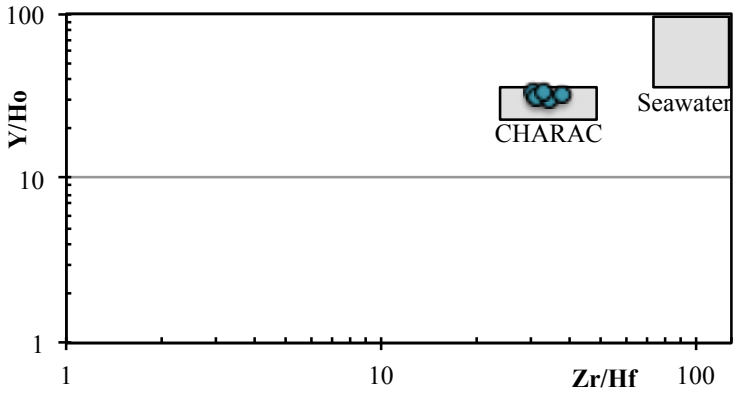

Figure 4: Zr/Hf versus Y/Ho ratios from the non-carbonate content are lower than the typical ratio values for seawater and scatter closely to the chondritic ratios and the CHARAC (Charge and Radius Controlled) field (after Bau, 1995)

Method	MDL	Analyte	Unit	Sample ID										
				1UF	2UF	3UF	4UF	5UF	6WF	7WF	8WF	10WF	11WF	12UF
			KG	0,02	0,04	0,07	0,04	0,03	0,03	0,03	0,05	0,02	0,02	0,02
LF200	0,01	SiO2	%	10,81	6,81	8,1	8,02	8,9	9,04	8,81	9,26	8,99	8,75	8,93
LF200	0,01	Al2O3	%	1,69	0,44	0,55	0,58	0,58	0,58	0,57	0,63	0,65	0,64	0,69
LF200	0,04	Fe2O3	%	0,34	0,22	0,22	0,27	0,24	0,22	0,24	0,23	0,23	0,24	0,28
LF200	0,01	MgO	%	0,41	0,27	0,26	0,26	0,26	0,26	0,26	0,27	0,27	0,27	0,28
LF200	0,01	CaO	%	46,17	49,66	47,96	48,06	47,69	47,85	47,89	47,8	48,24	48,37	47,62
LF200	0,01	Na2O	%	0,33	0,14	0,15	0,15	0,16	0,16	0,14	0,16	0,14	0,14	0,14
LF200	0,01	K2O	%	0,19	0,07	0,09	0,09	0,09	0,09	0,08	0,09	0,09	0,09	0,1
LF200	0,01	TiO2	%	0,03	0,01	0,02	0,02	0,02	0,02	0,02	0,02	0,02	0,02	0,02
LF200	0,01	P2O5	%	0,09	0,07	0,09	0,09	0,09	0,09	0,09	0,1	0,09	0,09	0,1
LF200	0,01	MnO	%	0,1	0,1	0,09	0,09	0,09	0,09	0,09	0,1	0,09	0,09	0,09
LF200	0,002	Cr2O3	%	<0.002	<0.002	<0.002	<0.002	<0.002	<0.002	<0.002	<0.002	<0.002	<0.002	<0.002
LF200	20	Ni	PPM	<20	<20	<20	<20	<20	<20	<20	<20	<20	<20	<20
LF200	1	Sc	PPM	4	<1	<1	1	<1	<1	<1	1	1	1	2
LF200	-5,1	LOI	%	39,6	42	42,3	42,2	41,7	41,4	41,6	41,2	41	41,1	41,6
LF200	0,01	Sum	%	99,8	99,81	99,83	99,81	99,83	99,83	99,83	99,82	99,82	99,83	99,82
LF200	1	Ba	PPM	182	113	121	122	127	123	126	129	126	127	135
LF200	1	Be	PPM	<1	<1	<1	<1	<1	<1	<1	<1	<1	<1	<1
LF200	0,2	Co	PPM	5,1	1,3	1,7	2,8	1,8	2,1	2,2	2,3	2,6	2,7	3,2
LF200	0,1	Cs	PPM	0,4	0,1	0,1	0,2	<0.1	0,2	0,2	0,1	0,2	<0.1	0,2
LF200	0,5	Ga	PPM	1,5	<0.5	<0.5	<0.5	<0.5	<0.5	<0.5	<0.5	<0.5	<0.5	<0.5
LF200	0,1	Hf	PPM	0,3	<0.1	<0.1	<0.1	<0.1	0,1	0,1	<0.1	0,1	0,1	0,1
LF200	0,1	Nb	PPM	0,9	0,2	0,5	0,5	0,4	0,3	0,4	0,4	0,4	0,4	0,4
LF200	0,1	Rb	PPM	6,5	2,4	3,2	3,2	3,2	3,2	3,1	3,3	3,6	3,4	3,4
LF200	1	Sn	PPM	<1	<1	<1	<1	<1	<1	<1	<1	<1	<1	<1
LF200	0,5	Sr	PPM	1197	1268,1	1097,4	1161,9	1152,9	1144	1113,2	1147,1	1159,7	1166,7	1145,3
LF200	0,1	Ta	PPM	<0.1	<0.1	<0.1	<0.1	<0.1	<0.1	<0.1	<0.1	<0.1	<0.1	<0.1
LF200	0,2	Th	PPM	0,7	0,4	0,4	0,3	0,6	0,5	0,5	0,5	0,5	0,4	0,6
LF200	0,1	U	PPM	0,2	0,2	0,2	0,2	<0.1	0,1	0,2	0,2	0,2	0,1	0,2
LF200	8	V	PPM	20	<8	<8	9	<8	10	9	8	10	8	11
LF200	0,5	W	PPM	<0.5	<0.5	<0.5	<0.5	<0.5	<0.5	<0.5	1	<0.5	<0.5	<0.5
LF200	0,1	Zr	PPM	6,5	2,8	4,7	4,2	4,4	4,6	4,3	5	5,1	4,6	4,9
LF200	0,1	Y	PPM	13,60	11,30	10,20	11,30	12,10	12,10	10,80	11,90	12,60	11,70	11,90
LF200	0,1	La	PPM	13,40	10,80	10,60	10,70	12,10	11,20	11,20	12,20	11,70	11,70	12,20
LF200	0,1	Ce	PPM	16,30	11,20	11,20	11,30	11,50	12,50	11,90	12,70	12,90	12,50	12,50
LF200	0,02	Pr	PPM	2,88	2,07	2,04	2,17	2,24	2,25	2,19	2,30	2,42	2,41	2,46
LF200	0,3	Nd	PPM	11,70	8,40	8,10	7,90	9,10	9,70	9,10	10,00	9,50	10,60	10,10
LF200	0,05	Sm	PPM	2,40	1,54	1,49	1,63	1,73	1,92	1,60	1,87	1,74	1,94	1,85
LF200	0,02	Eu	PPM	0,58	0,39	0,40	0,40	0,43	0,41	0,47	0,43	0,44	0,50	0,42
LF200	0,05	Gd	PPM	2,48	1,95	1,80	1,91	1,93	1,92	1,93	1,94	2,14	2,09	2,12
LF200	0,01	Tb	PPM	0,40	0,31	0,25	0,26	0,28	0,28	0,29	0,29	0,30	0,29	0,31
LF200	0,05	Dy	PPM	2,01	1,49	1,45	1,45	1,71	1,62	1,50	1,72	1,64	1,70	1,86
LF200	0,02	Ho	PPM	0,42	0,28	0,27	0,31	0,33	0,35	0,32	0,33	0,33	0,34	0,33
LF200	0,03	Er	PPM	1,33	0,91	0,79	0,80	0,88	0,87	0,90	0,88	0,97	0,97	0,94
LF200	0,01	Tm	PPM	0,18	0,12	0,11	0,11	0,12	0,13	0,13	0,15	0,14	0,13	0,14
LF200	0,05	Yb	PPM	1,06	0,71	0,70	0,77	0,72	0,69	0,68	0,71	0,77	0,83	0,81
LF200	0,01	Lu	PPM	0,14	0,10	0,09	0,11	0,11	0,11	0,09	0,11	0,12	0,11	0,11
TC000	0,02	TOT/C	%	10,92	12,79	14,48	14,1	13,63	13,17	13,46	13,28	13,03	12,84	13,14
TC000	0,02	TOT/S	%	0,04	0,02	0,03	0,04	0,03	0,04	0,03	0,03	0,03	0,04	0,07
AQ200	0,1	Mo	PPM	<0.1	<0.1	<0.1	<0.1	<0.1	<0.1	<0.1	<0.1	<0.1	<0.1	<0.1
AQ200	0,1	Cu	PPM	4	1,6	2,5	3	2,4	3,7	4,2	3	3,8	4,1	3,2
AQ200	0,1	Pb	PPM	2,6	1,2	1,8	1,8	1,7	2,1	1,9	1,7	2,3	2,2	2,3
AQ200	1	Zn	PPM	29	5	9	100	6	8	9	5	9	11	59
AQ200	0,1	Ni	PPM	10,5	1,9	3,8	6,7	3,6	4,8	4,1	3,8	5,9	6,1	4,8
AQ200	0,5	As	PPM	<0.5	<0.5	<0.5	1	<0.5	<0.5	<0.5	<0.5	<0.5	<0.5	<0.5
AQ200	0,1	Cd	PPM	0,7	0,3	0,4	2	0,2	0,3	0,4	0,3	0,4	0,3	0,9
AQ200	0,1	Sb	PPM	<0.1	<0.1	<0.1	<0.1	<0.1	<0.1	<0.1	<0.1	<0.1	<0.1	<0.1
AQ200	0,1	Bi	PPM	<0.1	<0.1	<0.1	<0.1	<0.1	<0.1	<0.1	<0.1	<0.1	<0.1	<0.1
AQ200	0,1	Ag	PPM	<0.1	<0.1	<0.1	<0.1	<0.1	<0.1	<0.1	<0.1	<0.1	<0.1	<0.1
AQ200	0,5	Au	PPB	3,8	3,6	3	4,1	2,2	2,1	3,2	2,3	1	1,1	2,5
AQ200	0,01	Hg	PPM	<0.01	<0.01	<0.01	0,02	<0.01	<0.01	<0.01	<0.01	<0.01	<0.01	<0.01
AQ200	0,1	Tl	PPM	<0.1	<0.1	<0.1	<0.1	<0.1	<0.1	<0.1	<0.1	<0.1	<0.1	<0.1
AQ200	0,5	Se	PPM	<0.5	<0.5	0,5	<0.5	<0.5	<0.5	<0.5	<0.5	<0.5	<0.5	<0.5

PAAS
18
38
80
8,9
32
5,6
1,1
4,7
0,77
4,4
1
2,9
0,4
2,8
0,43

Figure 5: Overview of element concentrations in the whole-rock geochemistry analysis

Method	MDL	Analyte	Unit	Sample ID					
				1UF	2UF	12UF	9WF	10WF	
				Rock Pulp	Rock Pulp	Rock Pulp	Rock Pulp	Rock Pulp	
LF200	0,01	SiO2	%	74,96	66,87	66,78	72,04	72,07	
LF200	0,01	Al2O3	%	8,73	4,36	5,91	4,88	5,4	
LF200	0,04	Fe2O3	%	1,58	0,67	1,02	0,7	0,75	
LF200	0,01	MgO	%	1,16	0,61	0,82	0,65	0,69	
LF200	0,01	CaO	%	1,18	4,34	3,53	1,43	1,36	
LF200	0,01	Na2O	%	0,22	0,14	0,17	0,16	0,17	
LF200	0,01	K2O	%	1,14	0,65	0,77	0,72	0,78	
LF200	0,01	TiO2	%	0,21	0,12	0,15	0,14	0,15	
LF200	0,01	P2O5	%	0,53	0,56	0,64	0,62	0,64	
LF200	0,01	MnO	%	<0.01	<0.01	<0.01	<0.01	<0.01	
LF200	0,002	Cr2O3	%	0,005	0,004	0,003	0,004	0,003	
LF200	20	Ni	PPM	94	30	51	41	35	
LF200	1	Sc	PPM	4	2	3	2	2	
LF200	-5,1	LOI	%	10,2	21,6	20,1	18,6	17,9	
LF200	0,01	Sum	%	99,88	99,93	99,9	99,92	99,92	
LF200	1	Ba	PPM	212	155	180	192	177	
LF200	1	Be	PPM	2	<1	2	1	2	
LF200	0,2	Co	PPM	25,1	4,3	13,1	8,6	9,2	
LF200	0,1	Cs	PPM	2,1	1,2	1,1	1,2	1,2	
LF200	0,5	Ga	PPM	8,6	4,4	5,3	5	5,5	
LF200	0,1	Hf	PPM	1,1	0,8	1	1	0,9	
LF200	0,1	Nb	PPM	4,7	2,7	3	3,2	3,5	
LF200	0,1	Rb	PPM	39	20,4	25,2	24,1	25,8	
LF200	1	Sn	PPM	<1	<1	1	<1	<1	
LF200	0,5	Sr	PPM	96,6	187,2	166,2	119,4	113,5	
LF200	0,1	Ta	PPM	0,4	0,5	0,2	0,8	0,3	
LF200	0,2	Th	PPM	3,6	2,4	3,7	3,7	4	
LF200	0,1	U	PPM	0,7	0,7	1,2	1	1	
LF200	8	V	PPM	87	49	66	55	65	
LF200	0,5	W	PPM	1,3	1,3	2	1,6	1,4	
LF200	0,1	Zr	PPM	37,8	24,2	32,9	31,2	33,8	PAAS
LF200	0,1	Y	PPM	24,3	26,4	30,5	29,5	29,5	27
LF200	0,1	La	PPM	25,4	22,8	28,7	27,3	28,6	38
LF200	0,1	Ce	PPM	46,2	34,2	42,8	40,7	41,3	79,6
LF200	0,02	Pr	PPM	8,08	6,66	8,48	7,83	8,1	8,83
LF200	0,3	Nd	PPM	35,1	28,8	37,9	34,1	35,7	33,9
LF200	0,05	Sm	PPM	6,91	6,03	7,69	6,93	7,56	5,6
LF200	0,02	Eu	PPM	1,53	1,37	1,65	1,46	1,63	1,1
LF200	0,05	Gd	PPM	6,76	6,24	7,24	6,88	7,05	4,7
LF200	0,01	Tb	PPM	0,91	0,79	1,01	0,91	0,92	0,77
LF200	0,05	Dy	PPM	4,7	4,43	5,08	4,32	5	4,4
LF200	0,02	Ho	PPM	0,8	0,78	0,91	0,94	0,91	0,99
LF200	0,03	Er	PPM	1,81	1,92	2,21	2,27	2,27	2,9
LF200	0,01	Tm	PPM	0,22	0,23	0,25	0,24	0,25	0,4
LF200	0,05	Yb	PPM	1,24	1,35	1,46	1,31	1,42	2,8
LF200	0,01	Lu	PPM	0,16	0,16	0,2	0,18	0,18	0,43
TC000	0,02	TOT/C	%	5,02	16,2	14,53	13,98	13,44	
TC000	0,02	TOT/S	%	0,45	0,1	0,37	0,12	0,13	
AQ200	0,1	Mo	PPM	3	<0.1	0,5	0,2	0,2	
AQ200	0,1	Cu	PPM	38,1	20,2	36,7	36,1	30,7	
AQ200	0,1	Pb	PPM	20	5,8	12,8	8,1	8,3	
AQ200	1	Zn	PPM	419	22	134	36	82	
AQ200	0,1	Ni	PPM	568,4	22,6	44,4	37,6	33	
AQ200	0,5	As	PPM	133,3	2	5,6	2,4	2,1	
AQ200	0,1	Cd	PPM	6	0,5	3,4	0,9	1,7	
AQ200	0,1	Sb	PPM	1,2	0,2	0,4	0,2	0,2	
AQ200	0,1	Bi	PPM	0,1	0,2	0,3	0,3	0,2	
AQ200	0,1	Ag	PPM	<0.1	<0.1	<0.1	<0.1	<0.1	
AQ200	0,5	Au	PPB	83,1	0,8	3,7	1,4	1,2	
AQ200	0,01	Hg	PPM	0,24	0,02	0,04	0,03	0,03	
AQ200	0,1	Tl	PPM	2,4	<0.1	<0.1	<0.1	<0.1	
AQ200	0,5	Se	PPM	1,3	<0.5	<0.5	<0.5	<0.5	

Figure 6: Overview of element concentrations in the non-carbonate fraction

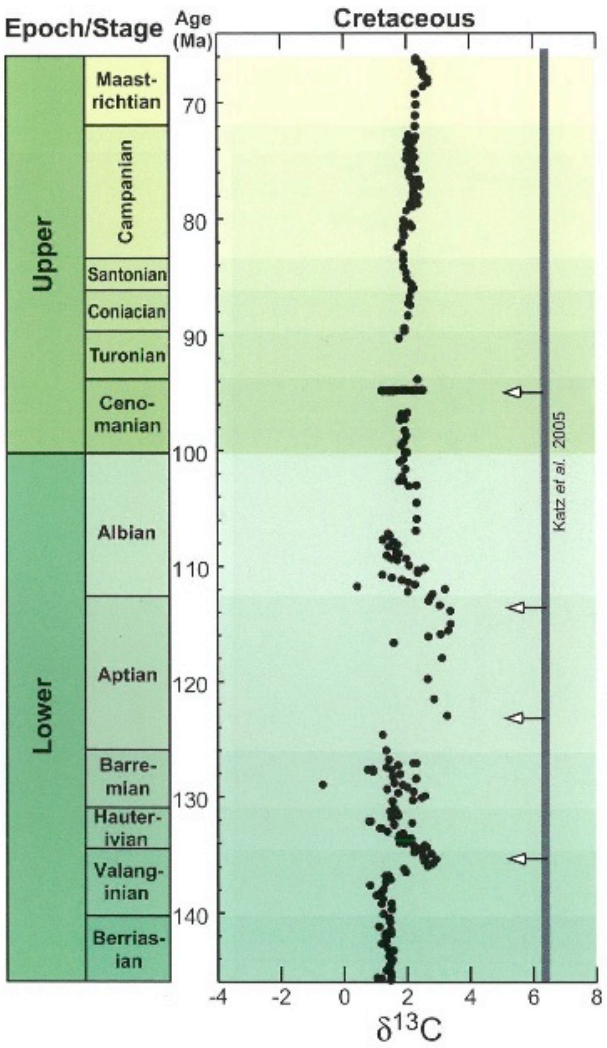

Figure 7: Variation of carbon ratios through Cretaceous, from Gradstein et al., 2012

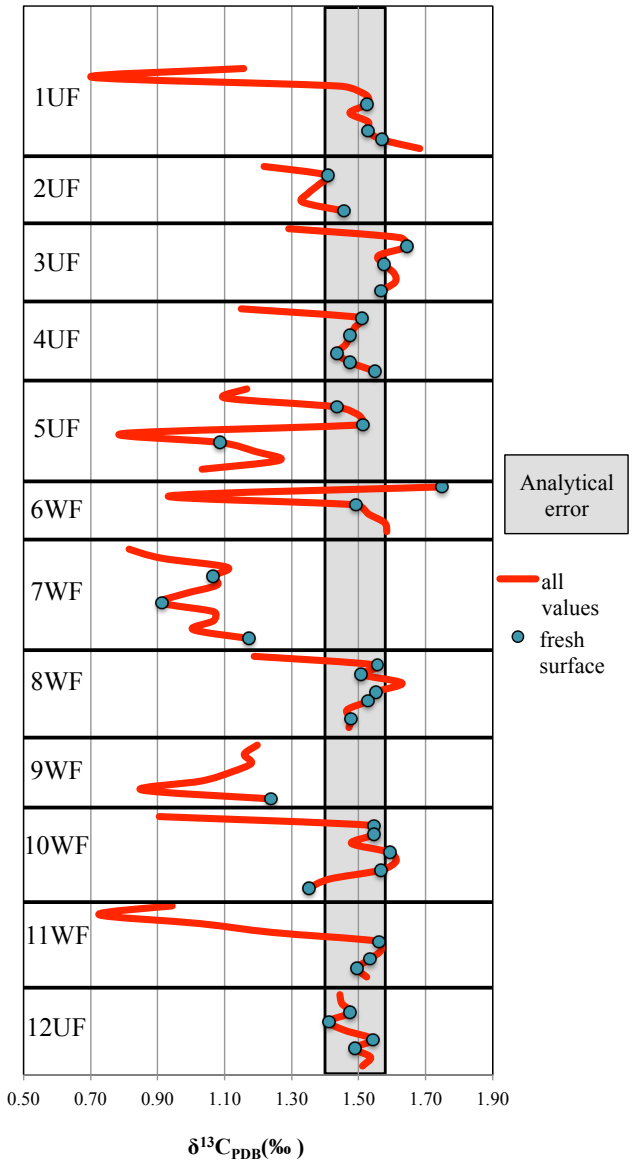

Figure 8: Carbon isotope ratios

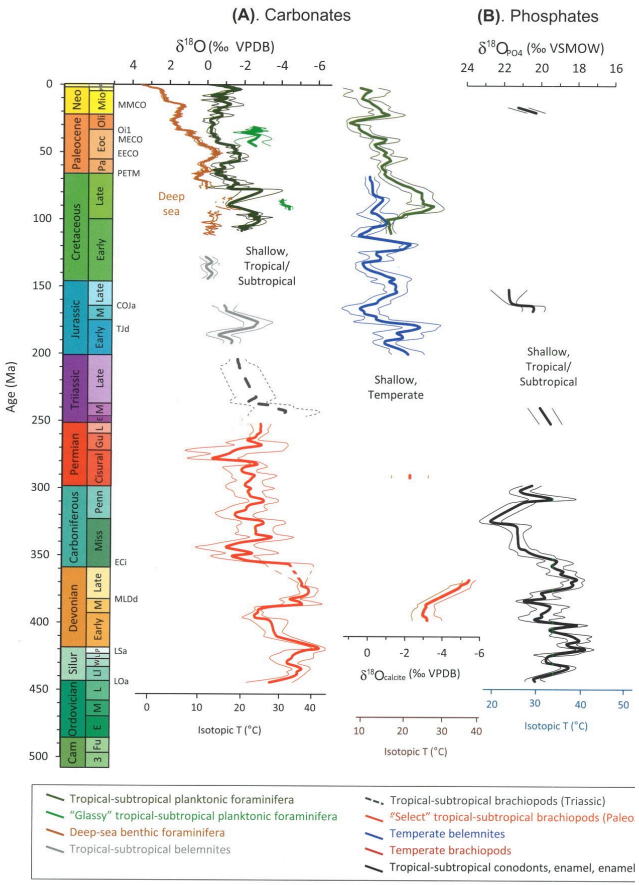

Figure 9: Oxygen isotopic stratigraphies for the Phanerozoic based on carbonates (A) and phosphate (B) from Gradstein et al., 2012

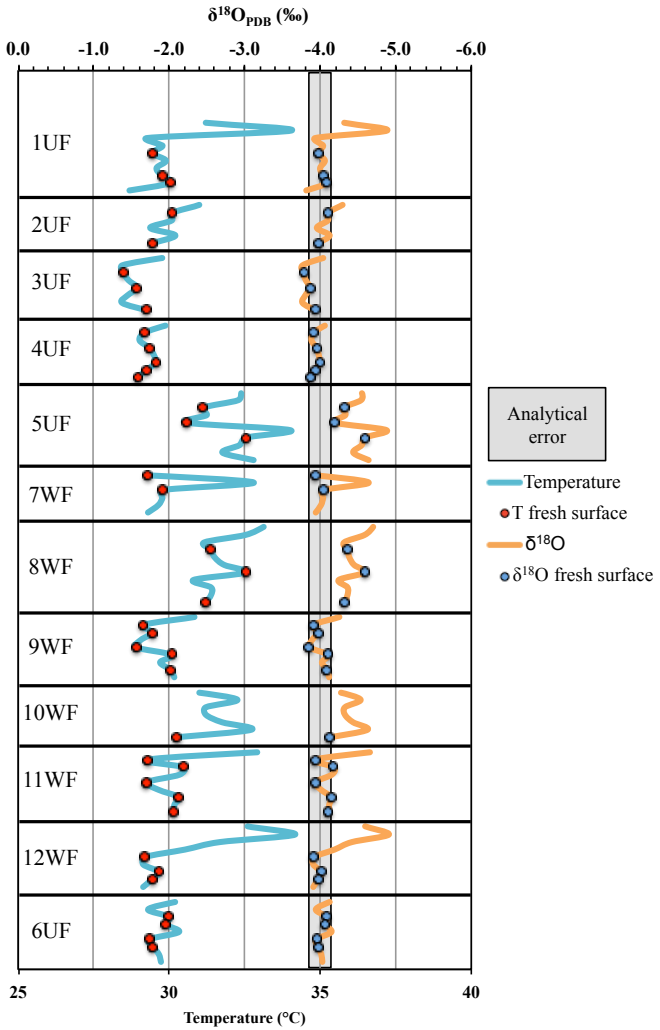

Figure 10: Oxygen isotope ratios and the calculated paleowater temperature